ANL-6810
Reactor Technology
(TID-4500, 26th Ed.)
AEC Research and
Development Report

ARGONNE NATIONAL LABORATORY
9700 South Cass Avenue
Argonne, Illinois 60440

REACTOR DEVELOPMENT PROGRAM PROGRESS REPORT

December 1963

Albert V. Crewe, Laboratory Director
Stephen Lawroski, Associate Laboratory Director

Division	Director
Chemical Engineering	R. C. Vogel
Idaho	M. Novick
Metallurgy	F. G. Foote
Reactor Engineering	L. J. Koch
Reactor Physics	R. Avery
Remote Control	R. C. Goertz

Report coordinated by
R. M. Adams and A. Glassner

Issued January 15, 1964

Operated by The University of Chicago
under
Contract W-31-109-eng-38
with the
U. S. Atomic Energy Commission

DISCLAIMER

FOREWORD

The Reactor Development Program Progress Report, issued monthly, is intended to be a means of reporting those items of significant technical progress which have occurred in both the specific reactor projects and the general engineering research and development programs. The report is organized in a way which, it is hoped, gives the clearest, most logical over-all view of progress. The budget classification is followed only in broad outline, and no attempt is made to report separately on each sub-activity number. Further, since the intent is to report only items of significant progress, not all activities are reported each month. In order to issue this report as soon as possible after the end of the month editorial work must necessarily be limited. Also, since this is an informal progress report, the results and data presented should be understood to be preliminary and subject to change unless otherwise stated.

The issuance of these reports is not intended to constitute publication in any sense of the word. Final results either will be submitted for publication in regular professional journals or will be published in the form of ANL topical reports.

The last six reports issued in this series are:

June 1963	ANL-6749
July 1963	ANL-6764
August 1963	ANL-6780
September 1963	ANL-6784
October 1963	ANL-6801
November 1963	ANL-6808

TABLE OF CONTENTS

TABLE OF CONTENTS

TABLE OF CONTENTS

I. BOILING WATER REACTORS

A. BORAX-V

1. Operations

The reactor was not operated during the month of December pending outcome of the examinations of the central superheater fuel assemblies.

Underwater inspection of the 12 irradiated central superheater fuel assemblies has been completed. This inspection included periscope observation of: (1) light passed through the length of the central portion of the fuel assembly coolant channels, enabling viewing of a $1\frac{1}{2}$-in.-dia circle which comprises about 15% of the coolant channel volume, and (2) the fuel plate bottom ends.

Prior to central superheater operation at zero power, the leaks that had been detected in the superheater fuel assemblies (see Progress Report for September 1963, ANL-6784, p. 1) had been repaired by fillet welds on the joints where the five fuel elements in each assembly are joined to the top and bottom flow vanes which maintain moderator gap spacing. All assemblies inspected showed some weld burn-through of these repair welds through the insulating tubes to the bottom of adjacent fuel-plate dead ends; none showed cooling-channel distortion or reduction of coolant-channel dimensions in the light test area or apparent bowing of the insulating tubes. One fuel assembly installed recently but not run at power showed no distortion of the fuel-plate bottom ends. Eight assemblies showed minor fuel plate bottom distortion, and three moderate distortion. Of the latter three, one (assembly C-1) had several outward small bulges at the ends of the insulating tubes, one a similar single bulge, and the third none. In fission product leak tests conducted previously, assembly C-1 had shown a positive indication of such leakage. The other fuel assembly (C-4) found to be leaking fission products showed only minor fuel-plate distortion.

The central superheater fuel, including two renovated spare assemblies, has been reloaded into the reactor. The three fuel assemblies known to be leaking fission products have been replaced. Critical experiments at room temperature are currently being performed in one quadrant of the boiler zone of central superheater core CSH-1 to determine the optimum water-to-fuel ratio and associated number of poison rods required in the boiler. The water-to-fuel ratio is being varied by changing the number and arrangement of water-filled flow rods in the boiling fuel assemblies.

2. Modification and Maintenance

Repair and modification of two standard and one instrumented spare central superheater fuel assemblies has been completed. All of the burned-through repair welds which tacked the fuel plate bottoms to the insulating tubes were removed to permit expansion of the fuel element as designed. To further assure open coolant channels, all were gaged, and three spacer combs were installed in the channels at the top and bottom of each 4-plate fuel element. The top riser and bottom nozzle were rewelded on each assembly and the welds dye-checked. The renovated assemblies were straightened, leak-tested, and inspected.

3. Hot Cell Examination of Damaged Superheater Fuel Assembly C-3.

Further hot cell examination of the damaged BORAX-V superheater fuel element C-3 (see Monthly Progress Report for November 1963, ANL-6808, p. 1) confirmed that the fuel-plate damage was caused by unintentional welding of the lower ends of some of the fuel plates to the insulating cans. One of these plates was welded for its entire width, sealing the insulating space between plate and can at this point. Immediately above the weld, the plate was bulged against its neighbors and the can bulged in the opposite direction. It is significant that the bulges extend the full width of the plate and can, but only 3.8 cm along the length of the element. This kind of failure suggests that the bulges were produced by longitudinal tensile and compressive stresses rather than by steam pressure in the insulating space.

A somewhat similar failure was found in another subassembly in which two of the four fuel plates were firmly welded to the cans. In a 13-cm-long area, the four-plate assembly buckled as a unit, bringing the outer plates alternately in contact with the left and right sides of the insulating can. Dark spots on the surface of the plates were located at the points of contact. There was no evidence of plate melting at the spots; rather, they seemed to be spots with heavier than usual oxide deposits.

The crack in the lower transition cone was sectioned and was found to be at the junction of the cone and a filler strip. It provided a passage for leakage of moderator water into the superheated steam. A similar 7.6-cm-long crack had also occurred at the same location on the opposite side of the fuel element. It was not noticed in the initial examination, probably because it was nearly closed. In both cases there was incomplete fusion of the welds.

The source of fission products released in the reactor appears to be from one of the two torn plates reported last month. A metallographic examination of a section through the tear showed that fuel particles are present. However, the tear does not extend up quite as far as the fully fueled portion

of the plate. Three other small breaks were confined to the bottom 1.3 cm of the plates. From radiographs taken during the manufacture of these plates it could be seen that these are all below the fuel-containing portion.

4. In-core Instrumentation Development

The fuel-temperature measurements obtained during boiling core B-2 operation (see Monthly Progress Report for March 1963, ANL-6705, p. 88) indicated that the calibration of the W-W/26% Re thermocouples employed may be affected by radiation damage, thermal cycling, or other causes. An experiment has been started to determine if any major calibration shifts occur in such thermocouples due to integrated fast neutron flux.

A capsule containing two chromel-alumel thermocouples and a W-W/26% Re thermocouple in an insulated stainless steel slug is being irradiated in EBR-I. The temperature of the samples is limited to that attained by neutron and gamma heating, and is estimated to be less than 600°F for the argon-filled thimble in which the thermocouples are installed. Preliminary data are now being analyzed.

II. LIQUID-METAL-COOLED REACTORS

A. General Fast Reactor Physics

1. ZPR-III

Experiments with the mock-up of the French reactor RAPSODIE continued. Fission ratios with both sealed and gas-flow fission counters were measured at the core center and radial edge. Reactivity worth measurements at the core center were also completed.

For the measurements of the central fission ratio, the central drawer in Half No. 1 of the reactor was modified to accommodate a fission chamber at the front. As the core is loaded with 8.03 in. (20.3 cm) of its total height of 14.06 in. (35.71 cm) in Half No. 1, the fissile material in the counters is located at approximately 0.9 in. (2.3 cm) from the midplane of the core. Both Kirn-type[1] and gas-flow[2] fission chambers were measured at this position. The data were normalized by use of BF_3 proportional counters located outside of the blanket and of a Kirn-type, U^{235} fission chamber at the core axial edge. With the counters loaded in the same manner in a core drawer of Half No. 1, the fission rates were determined in the 1-S-16 matrix position for the core edge fission ratios.[3] The calculated fission ratios obtained with these fission rates normalized to one of the BF_3 proportional counters are given in Table I. The fission ratios as obtained from data normalized to the remaining counters are presently being calculated.

Table I. Assembly 44, RAPSODIE, Central and Core Edge Fission Ratios

	Central		Edge	
Ratio	Kirn	Gas-flow	Kirn	Gas-flow
U^{238}/U^{235}	0.0756	0.0818	-	0.06
U^{233}/U^{235}	1.532	-	-	1.50
U^{234}/U^{235}	0.433	0.445	-	0.37
U^{236}/U^{235}	0.157	0.175	-	0.14
Pu^{239}/U^{235}	1.186	-	-	-
Pu^{240}/U^{235}	0.490	-	-	-
Pu^{240}/Pu^{239}	-	-	0.34	-

[1] F. S. Kirn, Neutron Detection with an Absolute Fission Counter, Paper SM-36/74, Symposium on Neutron Detection, Dosimetry and Standardization, IAEA, Harwell, England, December, 1962.

[2] W. G. Davey, A Critical Comparison of Measured and Calculated Fission Ratios for ZPR-III Assemblies, ANL-6617 (Sept 1962).

[3] ANL-6801, Reactor Development Program Progress Report, October 1963, Figure 1. Initial Loading of Rapsodie Experiment, Assembly 44.

Measurements of central reactivity worth were made by use of the two center columns of the 1-P-16 drawer. The samples, all 2 in. (5.08 cm) in length, represent a small sample worth on the axis of the core, extending ±1 in. (2.54 cm) on either side of the midplane of the core. The worths of these materials are given in Table II.

Table II. Assembly 44, RAPSODIE, Central Reactivity Worths of Small Samples

Material	Reactivity, Ih/kg
Aluminum	28.0
Stainless Steel (SS)	16.92
Boron-10	-6,180
Polymethylene	5,410
Enriched Uranium	478.9
Pu (1 w/o Al)	853.6 (Corrected for SS cladding)
U^{233}	905.3 (Corrected for aluminum cladding)

The changing temperature distribution in the core due to opening and closing the halves (with the heating resulting from plutonium) has presented a problem in comparing the perturbation due to each sample to the reference. These worths have been corrected for core temperature change by means of a core temperature coefficient of reactivity and a mean temperature which is considered to be preliminary. Extended operation to attempt to evaluate reactivity as a function of core temperature and/or distribution is scheduled for early January.

After completion of the worth measurements of small central samples, a remote reactivity sample changer for the large 2 x 2 x 1-in. samples was installed in the reactor and initially checked out. By means of this changer, the 1-P-16 drawer is remotely retracted from the assembly while the halves are closed; two of the samples are then automatically inserted in the front 2 in. of the drawer. The drawer is then re-inserted remotely into the reactor and the sample worth measured.

Although the changer eliminates the error in half closure and the problem of the effect upon the core temperature of opening the halves between samples, it has introduced a new temperature problem. From the start of the removal of a sample to the finish of the insertion of the next sample approximately 40 min elapses. During this time the central matrix tube of the reactor is in a varying void condition which perturbs the axial central temperatures of the reactor. This effect and the effect of the overall temperature change of the core due to the extended periods of time which the halves are closed during a series of these worth determinations will be examined during the temperature coefficient evaluations in January.

Table III. Central Reactivity Coefficients

Sample	Number of Pieces and Size, in.	Weight, gm	Reactivity Change,[a] Ih	Ih/kg	ZPR-III Results, Ih/kg
Pu^{239}	1 - 1/4 x 2 x 2	87.87	38.1 ± 0.6[b]	433.5 ± 6.8	
U^{235}	2 - 1/16 x 2 x 2	136.58	34.6 ± 0.6	253.3 ± 4.4	
U^{235}	4 - 1/16 x 2 x 2	272.95	74.0 ± 0.6	271.1 ± 2.2	259.6 ± 2.1
U^{238}	4 - 1/8 x 2 x 2	600.97	-7.7 ± 0.6	-12.7 ± 1.0	
U^{238}	8 - 1/8 x 2 x 2	1201.12	-15.0 ± 0.6	-12.5 ± 0.5	-12.3 ± 0.2
Stainless Steel	4 - 1/4 x 2 x 2	510.06	-7.5 ± 0.6	-14.7 ± 1.2	-14.6 ± 0.5
$B_4^{10}C$	8 - 1/4 x 1/2 x 2[d]	63.5	-121.6 ± 2.0[c]	-1915 ± 32	-1869.2 ± 16.1
$B_4^{10}C$ + Lucite	8 - 1/4 x 1/2 x 2[e]	63.5	-153.3 ± 2.3[c]	-2414 ± 36	
$B_4^{10}C$ + Lucite	8 - 1/4 x 1/2 x 2[f]	63.5	-172.2 ± 2.2[c]	-2712 ± 35	
Aluminum	2 - 1/4 x 2 x 2	86.77	-1.7 ± 0.6	-19.6 ± 6.9	
Aluminum	4 - 1/4 x 2 x 2	173.44	-3.1 ± 0.6	-17.9 ± 3.5	-16.8 ± 1.4
Al_2O_3	4 - 1/8 x 2 x 2	78.9	-1.9 ± 0.6	-24.1 ± 7.6	
Al_2O_3	8 - 1/8 x 2 x 2	157.44	-2.9 ± 0.6	-18.4 ± 3.8	
Tungsten	4 - 1/8 x 2 x 2	580.23	-13.9 ± 0.6	-24.0 ± 1.0	
Tungsten	8 - 1/8 x 2 x 2	1163.7	-28.7 ± 2.8	-24.6 ± 2.4	
Rhenium	1 - 1/2 x 2 x 2	633.1	-41.6 ± 0.6	-65.7 ± 0.9	
Rhenium	2 - 1/2 x 2 x 2	1270.3	-82.2 ± 2.0[b]	-64.7 ± 1.6	
B^{10}	2 x 2 x 1	29.20	-84.9 ± 0.3	-2908 ± 10	-3036 ± 35
B_4C	2 x 2 x 1	66.96	-21.7 ± 0.3	324.1 ± 4.4	
Beryllium	2 x 2 x 1	120	-3.06 ± 0.10	-25.5 ± 0.8	-17.8 ± 2.1
Bismuth	2 x 2 x 1	555.5	-1.88 ± 0.10	-3.38 ± 0.20	-4.47 ± 0.4
Carbon	2 x 2 x 1	103	-2.86 ± 0.10	-27.8 ± 0.9	-31.0 ± 2.7
Copper	2 x 2 x 1	552.43	-10.7 ± 0.10	-19.4 ± 0.17	
Chromium	2 x 2 x 1	220.73	-3.35 ± 0.10	-15.2 ± 0.5	
Hafnium	2 x 2 x 1	805.3	-38.9 ± 0.3	-48.3 ± 0.4	
Inconel	2 x 2 x 1	519	-9.4 ± 0.3	-18.1 ± 0.6	
Lithium	2 x 2 x 1	28.6	-3.68 ± 0.10	-128.7 ± 3.5	
Manganese	2 x 2 x 1	209.6	-3.28 ± 0.10	-15.6 ± 0.5	
Molybdenum	2 x 2 x 1	599	-14.7 ± 0.3	-24.5 ± 0.5	
Nickel	2 x 2 x 1	545.98	-10.34 ± 0.10	-18.94 ± 0.18	
Niobium	2 x 2 x 1	481.2	-14.9 ± 0.10	-31.0 ± 0.2	
Palladium	2 x 2 x 1	643.2	-29.7 ± 0.2	-46.2 ± 0.3	
Potassium	2 x 2 x 1	44.55	-0.92 ± 0.10	-20.7 ± 2.2	
Sodium	2 x 2 x 1	51.38	-0.73 ± 0.10	-14.2 ± 2.0	
Sulfur	2 x 2 x 1	63.10	-2.13 ± 0.1	-33.8 ± 1.6	
Silver	2 x 2 x 1	642	-50.7 ± 0.1	-79.0 ± 0.2	-73.7 ± 0.7
Tantalum	2 x 2 x 1	924.7	-41.3 ± 0.1	-44.7 ± 0.1	
Vanadium	2 x 2 x 1	183.67	-3.08 ± 0.10	-16.8 ± 0.54	
Zirconium	2 x 2 x 1	406	-4.7 ± 0.3	-11.6 ± 0.7	-13.1 ± 0.6

[a] An error of ±0.6 Ih was assigned as a best estimate of the reproducibility of the measurements made after the tables had been separated and closed and the control rods scrammed. When the sample changer was used, an error estimated at ±0.1 Ih was given to each of those measurements which were made through use of the linear portion of the control rod worth calibration curve. An error estimate of ±0.3 Ih was given each of those measurements which were made by use of the nonlinear sections of the control rod calibration. These estimates assume that the differential worth of the control rod is 6.0 Ih/cm.

[b] The plutonium sample consisted of 94.51% Pu^{239}, 5.11% Pu^{240}, and 0.38% Pu^{241}. No correction was made for the effects of Pu^{240} and Pu^{241}.

[c] Error includes uncertainty of total worth of calibrated rod No. 2 (±1.2%) plus the uncertainty in differential worth of rod No. 9 (±2.5%).

[d] Total volume of B_4C pieces was 2 $in.^3$.

[e] B_4C sandwiched between eight Lucite pieces which formed two 1/4 x 2 x 2-in. layers. Total volume of B_4C and Lucite was 4 $in.^3$.

[f] Eight B_4C pieces (each 1/4 x 1/2 x 2 in.) and eight Lucite pieces (each 1/4 x 1/2 x 2 in.) homogeneously mixed. Total volume of B_4C and Lucite was 4 $in.^3$.

By means of the sample changer, the worths of V, Ta, W, Nb, Zr, Mo, Fe, Ph-I, Ph-II, Al, SS, O (Al_2O_3 and Fe_2O_3), Na, and graphite have been measured. These worths will be reported after the temperature coefficient effect is evaluated.

All worth measurements were performed at subcritical reactor power levels.

2. ZPR-VI

An investigation of the effects of fuel bunching concluded the experiments with Assembly No. 1, an all-metal assembly with a U^{238}/U^{235} atom ratio of c. 7. The core was disassembled and the facility was prepared for Assembly No. 2, a 650-liter carbide system.

A number of central reactivity coefficient measurements were made with Assembly No. 1 by inserting samples of various materials in a 1-in.-deep void at the front of a central drawer. The void existed in the center of the core at the interface of the two halves in the stationary half. Some of the measurements were made by inserting the samples manually after separating the halves. Others were made with a remotely controlled sample changer. The latter gave greater precision because it was not necessary to open and close the halves, nor to scram the control and safety rods. The results are reported in Table III. For comparison, the central reactivity coefficient measurements obtained with Assembly No. 22 of ZPR-III are also given in the table.

a. Radial Edge Worths. Table IV contains the relative worth measurements of samples to void volume made in the front 1-in. of a core edge drawer. The radial distance to the sample center was 27.62 cm.

Table IV. Relative Worth Measurements of Samples to Void Volume in a Core Edge Drawer

Sample	Number of Pieces and Size, in.	Weight, gm	Ih	Ih/kg
Rhenium	2 - $\frac{1}{2}$ x 2 x 2	1270.3	7.7 ± 0.6	6.1 ± 0.5
Rhenium	1 - $\frac{1}{2}$ x 2 x 2	635.4	3.7 ± 0.6	5.8 ± 0.9
Tungsten	8 - $\frac{1}{8}$ x 2 x 2	1163.71	1.1 ± 0.6	1.0 ± 0.5
Tungsten	4 - $\frac{1}{8}$ x 2 x 2	580.22	0.8 ± 0.6	1.4 ± 1.0

3. ZPR-IX

The construction of the ZPR-IX facility has been completed, and the entire system has been tested. Operation of the critical facility now awaits the approval of the Safety Analysis Report.

Miscellaneous equipment required to facilitate certain experimental measurements, such as a corner separation indicator for the assembly counter traverse drive mechanism, is currently being fabricated and installed.

B. General Fast Reactor Fuel and Process Development

1. Fuel Jacket Development

a. Duplex Tubing. The duplex tube of Type 304 stainless steel and vanadium (see Progress Report for October 1963, ANL-6801, p. 12) has been processed to a final size of 0.442-cm (0.174-in.) ID x 0.047-cm (0.018-in.) wall. The tube was drawn with a ductile core to a 0.572-cm (0.225-in.) OD x 0.485-cm (0.191-in.) ID. After removal of the core and annealing of the tube the latter was sunk to the final size. Characteristics of the bond are being evaluated by nondestructive testing.

b. V-10 w/o Ti (TV-10) and V-20 w/o Ti (TV-20) Alloys. Short lengths of 0.57-cm (0.224-in.)-OD x 0.06-cm (0.025-in.)-wall tubing of TV-10 and TV-20 have been produced by drilling as-extruded bar stock and ironing and drawing to final size. A piece of TV-10 tubing approximately 41 cm (16-in.) long has been inspected by X-ray and ultrasonic techniques and found to be defect free. An additional 41-cm (16-in.)-long section of TV-10 and a 23-cm (9-in.)-long piece of TV-20 tubing have been produced and are currently being inspected.

Isochronal annealing studies of TV-10 and TV-20 material have been completed. Diamond-pyramid-hardness measurements have been taken, and metallographic examination is in process to verify hardness data so that stress-relieving and recrystallizing temperatures can be determined. Preliminary data on the cold-working behavior and the stress-relieving and recrystallizing temperatures for pure vanadium, TV-10, and TV-20 are presented in Tables V and VI.

Table V. Diamond Pyramid Hardness as a Function of Percent Cold Work*

	Percent Cold Reduction				
Material	0	20	40	60	80
Pure Vanadium	155	-	-	178	201
TV-10	173	238	238	224	264
TV-20	228	287	299	287	299

*Data taken on longitudinal samples.

Table VI. Stress-relieving and Recrystallization Temperatures*

Material	Stress Relieving Temp, °C	Recrystallization Temp, °C
Pure Vanadium	400	800
TV-10	600	900
TV-20	600	900

*Data taken on longitudinal samples.

2. Process Development for Fast Reactor Fuels

a. Skull Reclamation Process. Work has continued on the development of the skull-reclamation process for recovery and purification of fissionable material in melt-refining crucible residues (skull material). Twelve waste metal ingots from four earlier demonstration runs in the large-scale integrated equipment were individually melted and sampled for uranium and fission product analysis. Analysis of these samples is in progress.

A transfer tube, which is made of gun-drilled molybdenum-30 w/o tungsten rod and is heated by five electric heaters, has been used without difficulty in the large-scale equipment for 18 transfers of metal and salt solutions by pressure siphoning.

b. Advanced Processes. Development work has continued on the use of a ternary cadmium-zinc-magnesium alloy as a process medium for the processing of plutonium-bearing fast reactor fuels. Substitution of this ternary solvent for magnesium-zinc is expected to allow operation at lower temperatures, where acceptably low corrosion rates will allow use of stainless steel equipment.

The separations are based on differences in the distribution behavior of uranium, plutonium, and fission products in liquid metal-molten salt systems. Data have been obtained on the codistribution behavior at 600°C of praseodymium and uranium between the Cd-Zn-Mg liquid metal and a flux composed of 30 m/o NaCl-20 m/o KCl-50 m/o $MgCl_2$. These data show a marked shift of the praseodymium distribution toward the metal phase with increasing zinc concentration. It appears that separation of rare earths from uranium and plutonium in the ternary liquid metal solvent by molten salt extraction will be feasible.

Results have been obtained on the solubility of uranium as a function of temperature in the liquid cadmium-zinc-magnesium alloys, 60 a/o Cd-30 a/o Zn-10 a/o Mg, 50 a/o Cd-30 a/o Zn-20 a/o Mg, and

74 a/o Cd-6 a/o Zn-20 a/o Mg. At 700°C, uranium solubility values as large as 6 w/o were obtained in an alloy containing 30 a/o Zn. At 600°C, the maximum uranium solubility observed was 3.8 w/o (observed in an earlier run with Cd-20 a/o Zn-10 a/o Mg). Since the alloy composition region of current process interest has been clarified, the work on uranium solubility determinations has been ended.

The identification of solid phases in equilibrium with the liquid cadmium-zinc-magnesium-uranium systems at various temperatures has been continued. By metallographic examination of quenched samples, it was determined that in the higher temperature region of retrograde solubility, uranium metal was the only solid phase present. In the intermediate temperature region, uranium-zinc intermetallic compounds (probably both delta and epsilon) were identified as equilibrium solid phases. Uranium-zinc intermetallic compounds and UCd_{11} were found in the low-temperature region.

c. Materials and Equipment Evaluations. Although pressed-and-sintered tungsten crucibles have been very satisfactory for containing molten zinc alloy and halide salt systems, their size is presently limited by manufacturing capabilities to about 20 in. in diameter. A possible method of overcoming the size limitations and of reducing the expense of tungsten crucibles is by coating less expensive materials with tungsten.

A tungsten-coated silicon carbide crucible ($10\frac{1}{2}$ in. in OD by 15 in. high) has successfully contained three individual charges of 50 w/o magnesium-zinc solutions, two of 5 w/o magnesium-zinc-uranium, and one of a halide salt system at 800°C for periods of one hour with mixing. There was no indication of any deleterious effect on the tungsten coating.

The tungsten coating on a stainless steel crucible of similar size had begun to crack and peel after being used to contain two charges of the 50 w/o magnesium-zinc solution at 800°C for 1 hr with mixing.

C. EBR-I, MARK IV

Experiments were continued to determine the effect of the core tightening and clamping devices on the reactivity changes observed with different modes of operation.

Seal plate shoes were retightened, but the magnitude of the reactivity change upon retightening was not the same as before they had been loosened (from the original condition). The changes observed were about 30 Ih, or midway between the 20 Ih noted with the shoes loose and the 40-Ih change measured prior to loosening (see Progress Report for November 1963, ANL-6808, p. 13).

The core clamps at the core centerline were then loosened two turns, or 0.026 in. across the core radius on the flats of the subassemblies. A loss of 50 Ih in reactivity was observed; this was regained when they were retightened. The reactivity changes observed after loosening the core clamps increased to about 55 Ih. After the core clamps were retightened, the changes were about 30 Ih, similar to those prior to loosening of the core clamps. However, with no further changes in the reactor conditions, the magnitude of the reactivity changes increased after about a week of operation to about 45 Ih, about the same as before any changes were made in the reactor clamping devices.

D. EBR-II

1. Reactor Plant

The wet critical experiments were completed on December 5, 1963. During the final phase of the experimental program, an inner blanket foil subassembly was irradiated for 4 hr at a power level of about 1 kW at a temperature of 460°F. The primary tank temperature was then increased to 550°F, and additional temperature coefficient data were obtained. A least-squares fit to the data collected at 600°F, 550°F, 500°F, and 460°F gave a temperature coefficient of 1.01 Ih/°F over the temperature range.

The discrepancy between foil-analysis data obtained in Idaho and at Argonne, Illinois (see Progress Report for November 1963, ANL-6808, p 15) has been resolved, and the data are now in good agreement

The worth of a control rod containing a boron poison section, as well as an enriched uranium section, was measured relative to a standard control rod in a "corner" control rod position at 550°F.

At the end of the experimental program, sufficient fuel was unloaded from the reactor to assure subcriticality by more than 1% $\Delta k/k$ even if the control and safety rods were fully inserted and the primary tank cooled to 200°F.

Eight enriched uranium inner blanket subassemblies were transferred from Row 6 of the reactor to the storage basket; they were replaced with depleted uranium subassemblies. One enriched uranium core subassembly was transferred from Row 4 to the storage basket and replaced with a natural uranium subassembly.

It has been calculated that the reactor would be subcritical by 3.3% $\Delta k/k$ with all control and safety rods up (fully inserted) at 600°F. The estimated subcriticality at 200°F would be 2.3% with all control and safety rods up; 6.4% with all control rods down (out of the core) and safety rods up; and 7.7% with all control and safety rods down.

The boron control rod was removed from the reactor. Because of malfunction of the fuel gripper described below, it was not possible to replace it with a standard control rod

The gripper shaft was sticking in the reactor vessel cover. The gripper was successfully freed by slight motion of the reactor vessel cover, indicating that the interference probably occurs between the shaft and some element of the cover. Investigation is proceeding to determine whether the gripper should be moved from the primary tank.

After initial alignment of the interbuilding coffin beneath the fuel-unloading machine, two dummy core subassemblies and four natural uranium core subassemblies were transferred from the storage basket to the Fuel Cycle Facility via the fuel-unloading machine and the interbuilding coffin. The subassemblies were cleaned in the coffin. After each subassembly transfer, except the last, the coffin was dried and returned to the reactor building.

Cool-down of the primary tank bulk sodium was begun on December 6. The freight door was opened, and components for removal of the second primary sodium pump were brought into the reactor building. The sodium temperature was lowered to 260°F and is being maintained around this temperature.

On December 17, primary sodium pump No. 2 was removed, because of failure by a procedure similar to that described in the Progress Report for June 1963, ANL-6749, p. 7. No temporary shielding plug was placed in the tank nozzle. After the silo was removed, a backing seal plate was secured to the transition piece.

The pump was allowed to cool in the argon atmosphere of the silo (cylindrical shell) for 12 hr. Dry air was then added slowly until the oxygen concentration was about 4%. The backing plate was secured to the bottom of the silo, and the pump and silo assembly were transferred from the transition piece to the operating floor, where more dry air was added for about 15 hr. The pump was then lowered out of the silo into a polyethylene bag, and cleaning and disassembly was started.

Preliminary inspection indicates that the No. 2 pump failure was similar to that of the No. 1 pump, namely, that the pump shaft galled with the lower aluminum bronze labyrinth.

The new shaft, with impeller assembled, was received for primary sodium pump No. 1, and this pump is being reassembled.

After removal of primary pump No. 2, the sodium surface in the primary tank was viewed through special windows in the transition piece trap door. The surface was very smooth, and light areas of sodium were seen between darker areas which appeared to be a very thin oxide film.

Rework of the steel floor plates and beams above the "depressed area" was begun. This is required to make room for a higher surge tank in the primary sodium purification system.

2. Sodium Boiler Plant

At the beginning of the month, all the secondary sodium was in the storage tank at a temperature of 600°F; the plugging temperature of the sodium was approximately 500°F. The secondary sodium and steam systems were at ambient temperature. Although the high pressure drop across the crystallizer tank of the cold trap prevented operation at a flow rate greater than an indicated 1 gpm, the cold trap was kept in service. The plugging temperature of the sodium in the storage tank was reduced to less than 300°F. During this operation, a sodium leak occurred in the bellows of the cold-trap bypass valve, resulting in a small fire. The bonnet and bellows assembly was replaced and the valve put back in service. The damaged assembly was cleaned and sent to Argonne, Illinois, for investigation of probable cause of failure.

Starting on December 6, the secondary sodium system and the steam system were heated to 350°F. The secondary system was filled on December 11, and the temperature was slowly raised to 567°F, where it has remained. During this heat-up, the plugging temperature rose more slowly than during previous runs, taking about a week to reach 500°F, whereas previously it had taken only about 2 days. Also, the plugging temperature has not risen above approximately 500°F, whereas during previous heat-ups it continued to rise. The cold-trap operation has been maintained, but the high pressure drop across the crystallizer tank has limited the flow to an indicated $\frac{1}{4}$ gpm. The temporary cold trap in the yard piping remained plugged during this run. Because some of the drain line temperatures are below the plugging temperature, the lines have been flushed once each shift to prevent oxide plugging.

The cold trap previously used in the temporary primary purification system was moved from the reactor building to the Sodium Boiler Plant and is being installed in the mixing line to the storage tank. A magnetic trap, fabricated in Argonne, Illinois, was also included in this installation. These components have not been put in service because of difficulties with the NaK cooling system for the cold trap.

A second small sodium fire occurred when the bellows of a sampling valve in the plugging indicator loop leaked. Replacing the bellows corrected the leak.

With the system at 570°F, thermal pipe deflection measurements were completed.

A successful full load test was run on the secondary electromagnetic pump to determine thermal equilibrium of the motor-generator set and pump windings. Additional work is required before the flowmeters and other sodium instrumentation are completely calibrated.

3. Power Plant

In early December the Power Plant systems were in shutdown condition, and the steam generator was in wet lay-up, completely filled with water chemically treated for corrosion inhibition. On December 6, heat-up of the steam generator and the secondary sodium system was started, as described above.

In conjunction with secondary sodium system clean-up, steam drum level was maintained by intermittent addition of feedwater to replace losses.

Some checkout, maintenance, and modification jobs were accomplished during the month. Cooling tower fans were checked, and some minor difficulties in the control circuits were corrected. It was discovered that inadvertent starting of the motor-driven feedwater pump, with the start switch at the feedwater control panel locked out, was possible by turning the selector switch to the "automatic" position. To provide temporary protection against this, the dc supply to the breaker has been interrupted; to afford permanent protection, the selector will be put under the control of a lock and key, as is the "start-stop" switch.

Load testing of the auxiliary heating boilers was performed, utilizing the turbine condenser. Condenser vacuum was established and the auxiliary boiler was loaded by passing steam through the main turbine bypass line. This bypass system contains the back-pressure regulating valves and the desuperheating section of the condenser which was used for the first time.

This operation required the use of the desuperheating sprays. Subsequent inspection of the strainers upstream of the spray nozzles revealed considerable debris in the strainers, which indicates that they are affording worthwhile protection to the nozzles.

Work has been started on the installation of the turbine lubricating oil transfer pump and the oil purification system.

4. Fuel Cycle Facility

The procedure for the removal of sodium from reactor fuel assemblies inside the interbuilding coffin by oxidation, hydrolysis, and washing was initially tested. Two dummy core assemblies and four natural uranium core assemblies were processed successfully at the sodium-removal station in

the Fuel Cycle Facility passageway. No difficulties were encountered during the runs; the cleaning appeared to be adequate, as judged by subsequent examination. Analysis of the wash water showed that initially 30-41 g of sodium were present on each assembly.

The dismantling machine was used to process further one of the natural uranium assemblies from which sodium had been removed in the coffin. Operation was generally satisfactory, except for an improper setting of the cutter at the position for separation of the lower blanket from the lower stainless steel section, and difficulty in shearing the tie bolts in the blanket section. The first problem has since been rectified.

More than 200 depleted uranium alloy fuel elements were decanned successfully in further in-cell testing of the decanning machine. Improved operation of the scrap cutter resulted from the use of heating units to raise the temperature of the machine, although some difficulty was encountered in feeding scrap to the cutter. Modifications to the scrap separator tube and fuel chopper orifice aimed at eliminating jamming were tested, but improvement was not clear-cut. Since it appeared that sodium-wetting difficulties were more of a problem with a high content of water vapor in the cell atmosphere, tests were conducted at various levels of moisture up to about 60 ppm, but marked improvement was not observed.

Four additional melt-refining runs in the Argon Cell were made to prepare ingots for subsequent operations. Pouring yields of uranium-fissium alloy were in the vicinity of 95%. A number of injection casting runs were completed in studies to determine optimum process conditions. Yields of castings more than 15 in. long were improved as the accumulator pressure was increased, and a maximum value of 99% was achieved. A second melt-refining furnace has been installed in the Argon Cell.

Because of the step-to-step feeding difficulties at the Window No. 7 pin-processing station, one of the demolding units was provided with a separate stand which was installed at Window No. 5 along with the remainder of the second pin-processing station. At this point, a Model A sealed master-slave manipulator was installed to assist feeding operations. Preliminary tests indicate that operability has been improved considerably. Gaging stations are being realigned and equipped with a magnetic clutch

Tubes in an initial group of 19 fuel pin jackets were classified according to internal diameters, and each was loaded with the proper quantity of sodium in the argon atmosphere glovebox. After transferring the group into the Argon Cell, depleted uranium fuel pins and restrainers were inserted remotely, the units were processed at the settling station, and apparently satisfactory welding was effected in the cell. The canned elements were next returned to the air cell for bonding, which was effected for $2\frac{1}{2}$ hr at 500°C. The rods will next be autoradiographed for level determination. The stroke of the bonding machine did not appear to be as

long or as reproducible as is desired, and the actuating solenoid overheated in sustained operation with a magazine full of elements. To prevent sticking of elements in the magazine, a larger solenoid will be obtained, and the bottom fittings of the magazine will be modified.

The gear-reducer unit in one of the in-cell cranes was extensively damaged when an up-limit switch circuit failed, which resulted in the hoist block wedging between the hoist drum and the equalizer pulley. The wedging action subjected the gear-reducer unit and the hoist drum to the full stalling torque of the hoist motor and the impact from the motor armature through a gear reduction of 1700 to 1.

Corrective measures for protecting the in-cell cranes have been taken. A new limit relay with improved operating characteristics has replaced the original relay in the up-limit switch system. To prevent overloading of the hoist mechanism should there be a future malfunction in the up-limit switch system, a slip clutch for the hoist drive has been designed at Argonne. The clutch is designed so that only the clutch half of the drive motor will have to be changed. The clutch will be set to slip at a torque about 50% higher than that required for normal operation of the hoist (load acceleration included). This will prevent slippage, and hence wear, of the clutch during normal operations, and still provide protection against overloading of the hoist mechanism. Slip clutches have been ordered for the hoist drives of the three in-cell cranes.

A furnace design has been proposed for skull-oxide processing in which the shell (atmosphere enclosure) of the furnace would act as the susceptor for induction heating. The shell would be surrounded by a layer of insulation which could be removed. The induction heating coil would be located around the insulation. This arrangement would provide for better cooling of the induction coil than conventional designs (where the coil is within the atmosphere enclosure). It would also allow the crucible to be rapidly cooled by mechanically removing the insulation. A test is underway to determine the feasibility of the design.

E. FARET

1. Design Studies

The present Title II design plan will provide for the issuance of two major construction packages and one or more procurement packages. The design of Package A, which will be comprised of the following major elements, is in progress:

a. access road, including culverts, base course, and suitable construction wearing course;

b. water and electrical power lines from EBR-II to terminal point at FARET site;

c. excavation for support wing and reactor building;

d. foundation preparation including check drilling, grouting, and foundation piers;

e. limited site grading compatible with structural excavation and drainage requirements;

f. all backfill which can be completed in this A package;

g. levelling slab for basement floors and foundations.

The design of the second construction package is planned for completion in December 1964 and will comprise the major construction package. Procurement packages will be developed as necessary in order to assure that equipment procurement will be made on a timely basis.

A site road and water line survey has been completed by the F. C. Torkelson Company. The purpose of this survey was to establish optimum routings based on actual field conditions and to provide information for design. Engineering drawings resulting from this study have been forwarded to the Architect for use in Title II design.

ANL and Bechtel engineers, concerned primarily with the electric power and the control and instrumentation aspects of FARET, met at the EBR-II site. The primary objectives of the visit were to familiarize these personnel with site conditions, the design features of the EBR-II, and Idaho Division experience which will affect or could be useful in the Title II design. Particular emphasis was placed on considerations which will affect selection of equipment, systems design and, to a certain extent, operating conditions.

General reviews and coordination of the Title II design by the Laboratory for the past month cover the following areas:

a. The feasibility of using ordinary concrete for shielding purposes was suggested. A study indicated that its use was desirable. Consequently, it is expected that ordinary concrete will be used for the cell ceiling and certain portions of the upper cell walls. This will result in economies in construction, but will not unduly affect overall plant operations.

b. Preliminary information concerning dry fuel storage criticality analysis, which will affect space arrangement and perhaps concrete design, have been transmitted to the Architect. The use of borated concrete in certain portions of the rear cell area related to fuel storage is being considered.

c. Reference dimensions of the reactor vessel which are required to develop construction Package A have been determined.

d. Shielding data of a preliminary nature concerning anticipated levels of radiation in various parts of the plant under a number of operating conditions have been developed, primarily for Laboratory use. This material includes multigroup neutron-flux estimates based on anticipated core designs and estimates of specific sodium activation in the primary coolant system. These data have been transmitted to Bechtel and should assist them in the development of the shielding design and help to expedite Title II work.

e. A number of typical specifications have been received from Bechtel for ANL consideration as to format, general language, and adequacy of depth of technical content. It is planned to evaluate these specifications from the requirements of both the Laboratory and Commission prior to finalizing specification format with Bechtel.

2. Safety Analysis

The draft of the Preliminary Safety Analysis Report has been completed and is being reviewed prior to submission to the Commission.

As part of the FARET safety study, a reactor meltdown problem has been coded for solution on the IBM-704 computer and has been designated as ANL-1891/RP. The code is used to investigate the dynamic behavior of a reactor for a positive reactivity insertion, and the corresponding positive and/or negative feedbacks arising from temperature-dependent effects and from the degree of core collapse after melting has started. The program essentially couples the dynamics of melting and collapsing of the core with the reactor kinetics equation.

The models used for the various changes in reactivity are incorporated into three basic types of reactivity insertions or feedbacks.

First is the externally applied reactivity: straight ramp insertions or ramp insertions up to a time t_0 may be allowed.

The second type of reactivity change considered is that which is a function of displacement, e.g., the collapsing of the core. The reactivity of collapse is determined from a series of static reactor calculations as a function of reactor height. The model used in these computations assumes that the melted segment of the fuel is uniformly distributed over the remaining core height with an equal volume displacement of coolant.

The time dependence of collapse is determined through a modified gravitational equation of motion, which allows the collapse to occur at an acceleration less than a "g." A "dynamic frictional" term is included to account for reactor designs involving closely packed fuel elements. An assemblage of melting fuel pins may behave quite differently than an isolated pin. (The coefficient can be estimated by performing experiments in TREAT on a cluster of pins.)

The third type of reactivity change considered is one which is dependent on the change of temperature, e.g., fuel and coolant expansion and Doppler effects. The code, at present, provides only the Doppler effect. The temperature dependence is taken from a series of static calculations involving Doppler-broadened cross sections for several fuel temperatures.

The code computes power and temperature distributions at each time interval. The time dependence of the reactor power, with one group of delayed neutrons, is computed by the usual neutron kinetics equations. The power distribution is assumed to have a cosine shape in the axial direction with a flat radial distribution. The core is divided axially into forty segments of equal size. When a segment melts and collapse occurs, the code recalculates the temperature distribution over the new height obtained by omitting the melted segment. The power and temperature at each time are used to compute the reactivity feedback through the equations defined above. The reactivity insertions are then fed back into the neutron kinetics equation.

Preliminary computations have been made for a series of positive reactivity-insertion rates ranging from \$3/sec to \$20/sec. Of particular interest are the results for the \$3/sec and \$5/sec cases, with and without the Doppler effect for the small core loading.

When the negative feedback of the Doppler coefficient is neglected, the time required to melt 87.5% of the core is 1.7 and 3.2 ms for the \$5/sec and \$3/sec ramp insertions, respectively. These are the shortest melting times involved and the net reactivity inserted is the largest.

The results of the meltdown computation indicate that for reactivity insertion rates below \$5/sec, the melting process starts some 200 to 300 ms after start of the external insertion. The time for 50% and 87.5% of the core to melt ranges from 1 to 10 ms.

It thus appears that the lower rates of external reactivity insertion lead to higher rates of insertion during the melting process because of the longer time available for acceleration of the molten fuel before significant pressure generation occurs.

To study this effect a series of computations were made with the introduction of negative Doppler coefficients of different magnitudes. The temperature-dependent negative feedback was introduced to compromise the initial positive insertion. The resulting rate of insertion found during the melting process confirms the conclusions stated for the non-Doppler case, that is, in the small-core case, a negative Doppler feedback would result in a greater reactivity contribution from the collapsing of the core. The magnitude of the Doppler is not large enough to effect a reactor shutdown. The effect of the negative feedback in this case is to increase the melting time and hence allow a greater degree of core collapse to occur.

3. Fuel Development

The UO_2 pellets for gas-gap fuel elements have been found to crack when subjected to heat fluxes of interest (see Progress Report for September 1963, ANL-6784, p. 27). Such cracking would likely lead to a decrease in the gap between pellet and clad and thus decrease the desirable fuel temperature conditions for the FARET Doppler experiment. Since UC has a much higher thermal conductivity than UO_2, the thermal stresses would be substantially smaller than in the oxide because of a lower temperature difference for a given heat flux. To determine the performance of UC pellets for gas-gap fuel elements, pellets were fabricated from nearly stoichiometric material which was wet milled, pressed at 20,000 psi, and sintered in vacuum (10^{-5} mm Hg pressure) for 4 hr at 1650°C. The compacts were found to have densities around 90 percent of theoretical. An electric-discharge machine was used to drill holes and finish exterior surfaces to required dimensions. The finished surfaces appeared poor due to fissures perpendicular to the cylindrical axis.

By means of a $\frac{1}{16}$-in.-OD tantalum resistance heater, located in the central axial hole of each of the pellets, the pellets were exposed ten times to a minimum and maximum heat flux of 2 and 20 W/cm. (The latter flux produces thermal stresses equal to those produced by a heat flux of about 33 W/cm in the reactor. A heat flux equivalent to 10 W/cm in the reactor appears to result in cracking of the pellets when fabricated of UO_2 material.) Each heat cycle lasted approximately one hour.

Table VII. Test Conditions for Uranium Monocarbide

Heat flux (W/cm)*	2	20
Clad Temp (°C)*	200	580
Carbide OD Temp (°C)**	280	865
Carbide ID Temp (°C)**	285	895

*Measured **Calculated

The test conditions are given in Table VII.

During the test, efforts were made to maintain the argon atmosphere at a low oxygen level by passing the argon gas through a heated manganous oxide bed before introduction to the test section.

Examination of the carbide pellets after the test (see Figure 1) showed that they retained their cylindrical shape. Pellets 1 and 6 were broken during disassembly of the test apparatus, pellet 4 was broken before assembly, and the crack in pellet 3 was thought to be the result of hammer blows during disassembly. There was no apparent indication of cracks resulting from the thermal cycling. Because of these encouraging results, additional tests will be made to determine the maximum heat flux that carbide pellets can withstand without cracking.

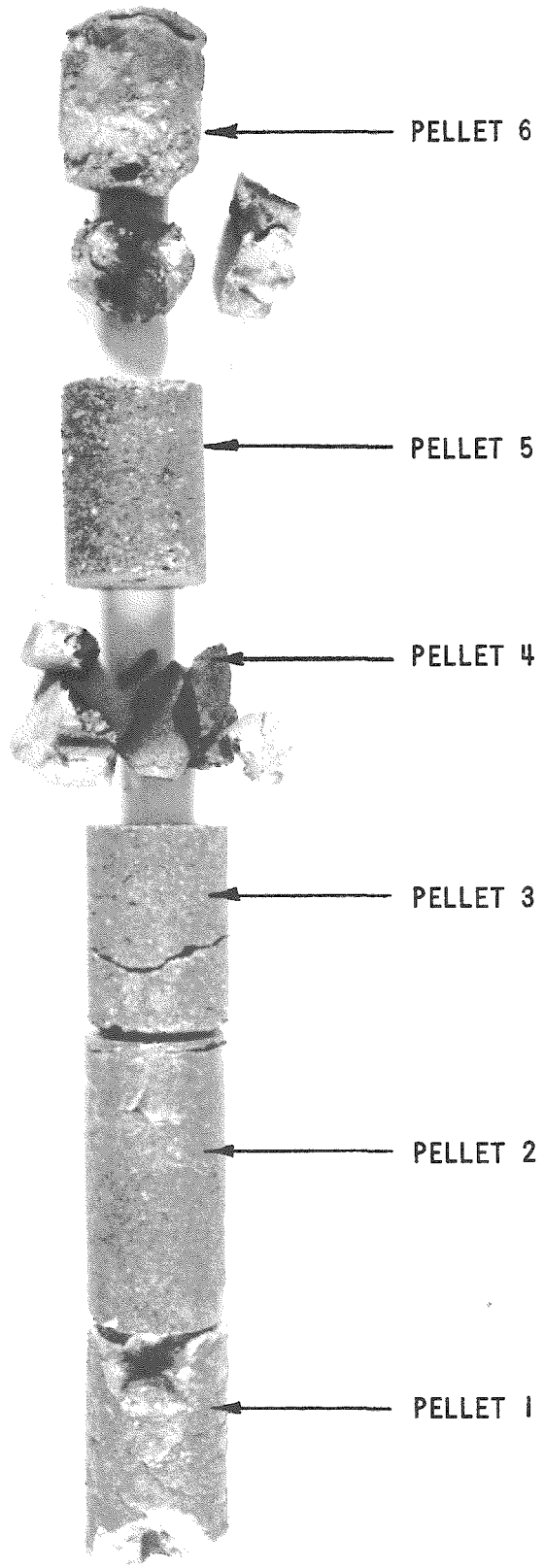

Figure 1. Uranium Carbide Pellets after Thermal Cycling

III. GENERAL REACTOR TECHNOLOGY

A. Applied Nuclear and Reactor Physics

1. Time-of-flight Experiments

a. Elastic Neutron Scattering. The results of measurements of differential elastic neutron scattering cross sections of cobalt, zinc, and copper have been prepared for publication. The measurements extend from incident neutron energies of 0.3 to 1.5 MeV. The experimental results are indicated in Figure 2, where the differential cross section is expressed in the series expansion

$$\frac{d\sigma}{d\Omega} = \frac{\sigma}{4\pi}\left[1 - \sum_{i=1}^{4} a_i P_i\right].$$

The incident neutron energy resolution was approximately 20 keV. Particularly in the case of cobalt, this energy spread was not sufficient to average over the resonance structure; thus the measured values tend to reflect the position and size of individual resonances (this is evident from the total cross section shown).

b. Inelastic Neutron Scattering. In conjunction with the above elastic measurements, the inelastic scattering cross sections of copper, cobalt, and zinc were determined. The inelastic excitations of levels in Cu^{63} at 668 and 961 keV, in Cu^{65} at 770 and 1114 keV, in cobalt at 1097 and 1189 keV, and in zinc at 990, 1040, and 1080 keV was observed. The results are given in Figures 3 and 4. Theoretical calculations are indicated by the points on each of these figures. The solid curves refer to Hauser-Feshbach calculations based on the general optical model parameters of Moldauer,[4] and the dotted lines indicate the result of applying corrections to the Hauser-Feshbach calculations to account for fluctuations in resonance effects. It is not clear from the experimental results that such fluctuation effects were observed.

c. Total Cross Sections. Total cross-section measurements by time-of-flight have been extended to the incident neutron energy range of 350 to 500 keV. Resolutions characteristically were of the order of 1 keV. Typical results for cobalt and iron are shown in Figure 5. Similar high resolution measurements have been made with fluorine, sulfur, and aluminum. These results were obtained with the use of an on-line data acquisition and processing which greatly expedited the research effort.

---

[4] P. A. Moldauer, Optical Model of Low Energy Neutron Interactions with Spherical Nuclei, Nuclear Physics 47(1), 65-92 (1963).

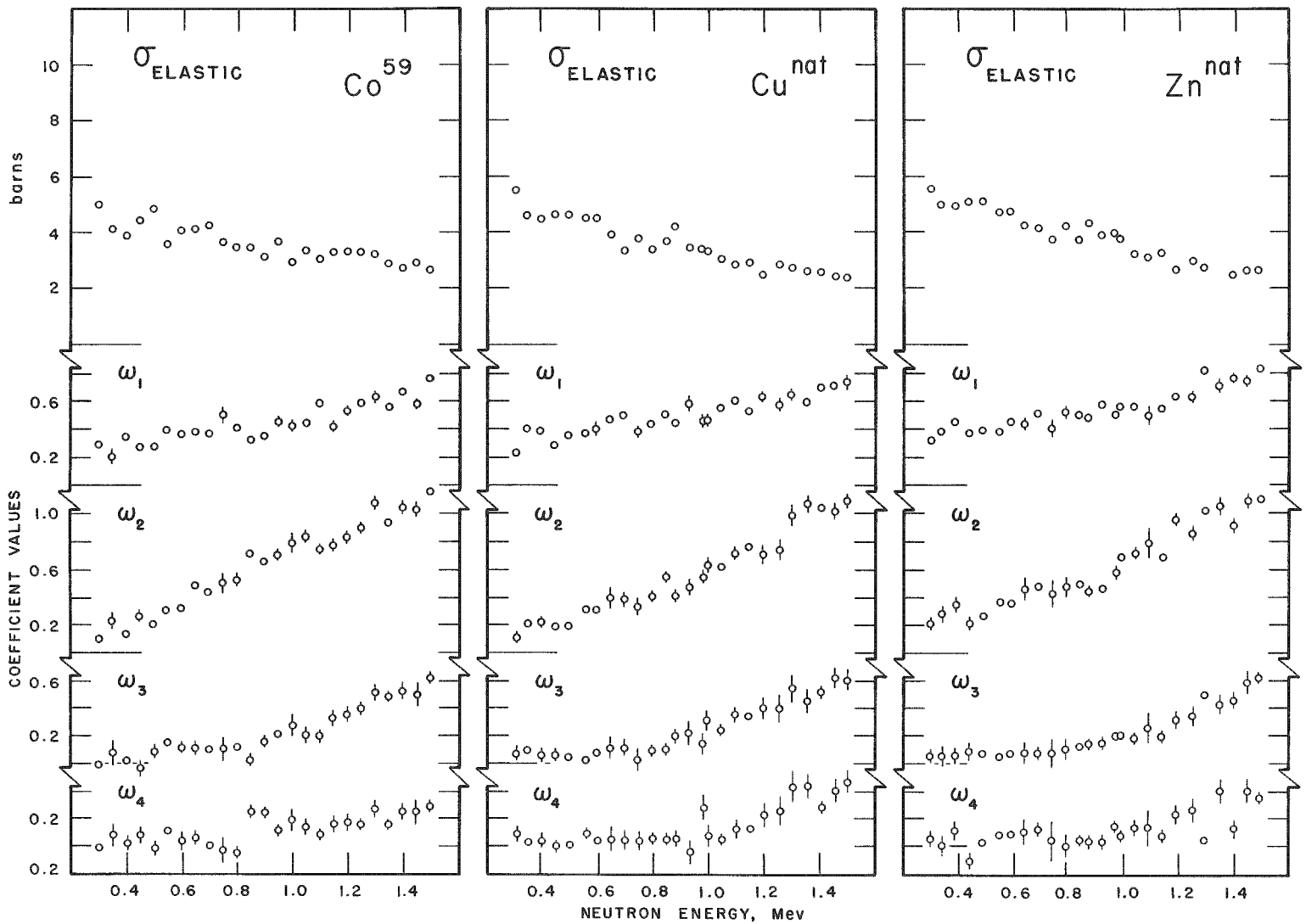

Figure 2. The Elastic Scattering Cross Section of Co, Cu, and Zn Expressed in the Form

$$\frac{d\sigma}{d\Omega} = \frac{\sigma}{4\pi}\left[1 + \sum_{i=1}^{4} \omega_i P_i\right].$$

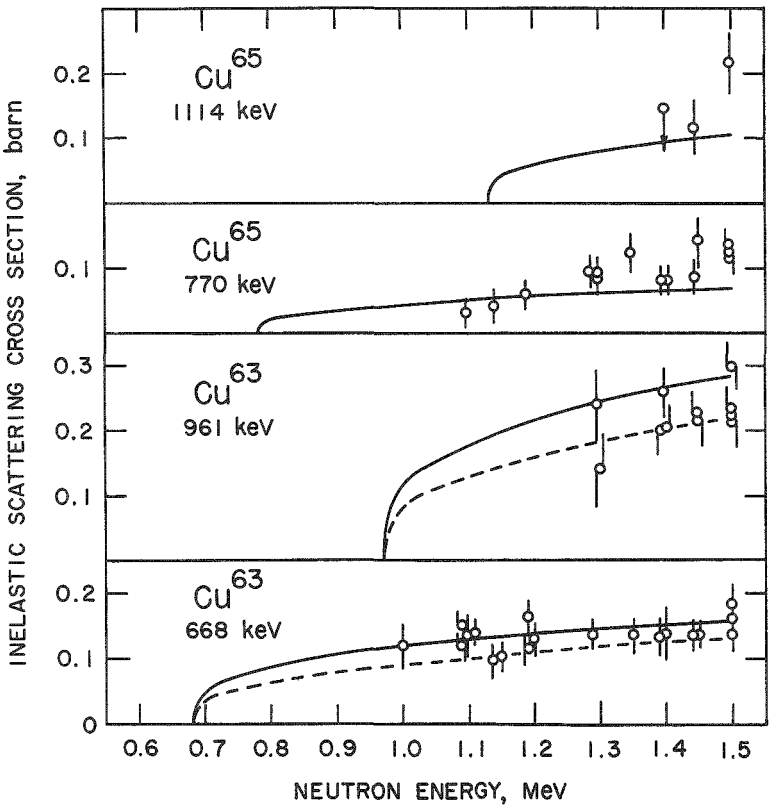

Figure 3

The Measured Inelastic Scattering Cross Section of Copper. The curves represent theoretical predictions and the points represent the experimental measurements.

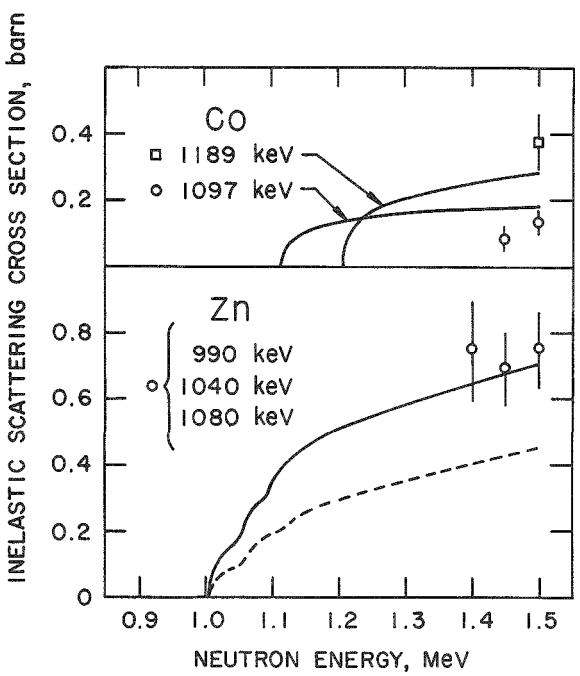

Figure 4

The Inelastic Scattering Cross Sections of Co and Zn. Curves represent theoretical predictions and the points represent the experimental measurements.

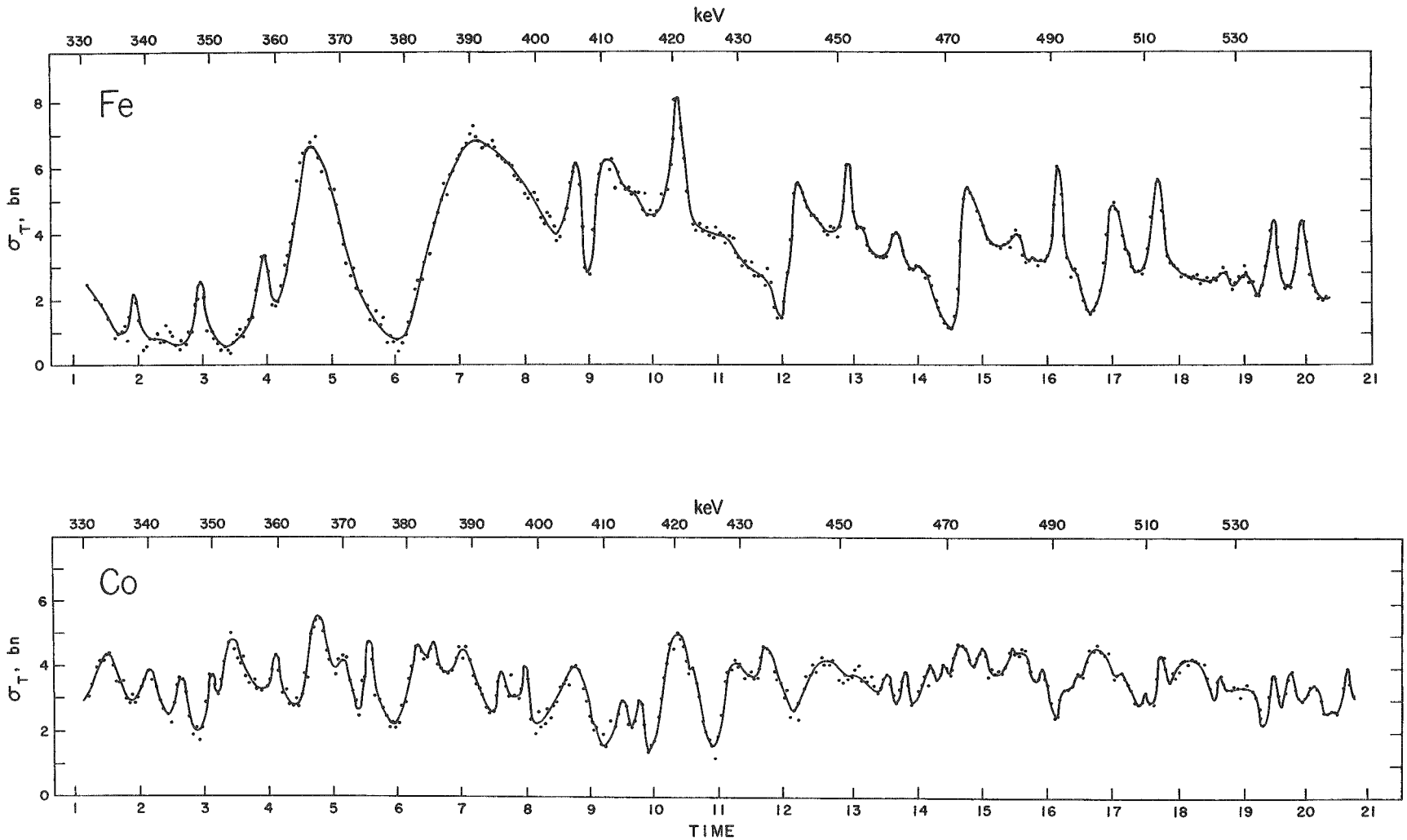

Figure 5. The Total Cross Sections of Fe and Co. Resolutions ~1 keV.

2. High-conversion Critical Experiments

Additional measurements were made with 3% enriched UO_2 fuel in a very heavily loaded lattice (see Progress Report for November 1963, ANL-6808, p. 33). A zoned core having a $H:U^{238}$ atom ratio of 0.99 ($H_2O:UO_2$ volume ratio ~0.33) was loaded in a 1.127-cm pitch triangular grid. A 10-cm-radius central zone contains stainless steel-clad fuel and is surrounded with a 18-cm-thick annular zone containing aluminum-clad fuel. An 8-cm-thick peripheral region in which alternate rows were left vacant (halving the fuel density) provides sufficient reactivity for criticality.

An initial conversion ratio (ICR) of 0.9 was measured in the central zone. This result agrees well with reported calculations.

It is expected that better accuracy will be achieved in future measurements. The precision, however, will be limited by mechanical tolerances. The fuel is so closely spaced that the clearance between fuel pins and grid openings permits local irregularities in moderator content which can affect results significantly. Another perturbation is introduced by the gap resulting from the insertion of foils between fuel pellets.

Radiochemical separation with absolute counting of selected fission product activities and neptunium decay are being carried out with UO_2 pellet samples. This should verify the foil measurements by an independent method.

Typical foil measurements gave the following results: cadmium ratio (Cd R) of U^{235} in fuel, 2.15 ± 0.05, and in the moderator, 2.3 ± 0.1; ratio of epi- to sub-cadmium fissions of U^{235} in fuel (ρ_f^{25}), 0.87 ± 0.04; the ratio of bare U^{235} foil activation in moderator versus fuel was 1.05 ± 0.01, indicating a thermal disadvantage factor near 1.1.

A triangular grid of 1.17-cm pitch should become available in January. This will permit loading a uniform lattice fuel zone having an atomic ratio $H:U^{238}$ of 1.3, which should be critical when loaded with the available aluminum-clad fuel (nearly 5,000 elements). This core should permit verification of data taken earlier with nonuniform loadings.

B. Theoretical Nuclear Physics

1. ZPR-VII Data Analysis

Calculations of the radial reflector savings were carried out for the Hi-C 1.24-cm square lattice with aluminum or stainless steel clad and the Hi-C, 1 27-cm triangular lattice with aluminum clad. Both two- and four-group calculations were done by means of the RE-122 diffusion theory code, with GAM-I constants for the non-thermal groups and

THERMOS constants for the thermal group. Calculated values of reflector savings, λ_R, agreed rather well with experimental values, the largest difference being around 3 mm.

Substitution of MUFT-4 constants for GAM-I constants in the first two groups of a calculation with three non-thermal groups for the Hi-C 1.24-cm aluminum-clad lattice led to a large decrease in reactivity (~5.7%). Much of this decrease is due to the fact that MUFT-4 constants show larger capture values in oxygen in group 1 and in U^{238} in group 2, and in smaller values of $\nu\Sigma_f$ in both groups. It was mentioned in ANL-6808 (Progress Report for November, 1963) that GAM-I constants led to reactivities which were 4 or 5% high for the Hi-C lattices.

2. Doppler Effect Studies

Effects of resonance overlapping on the Doppler broadening of fission and capture resonances of fissile isotopes have been studied extensively. A general expression, which includes the overlapping of neighboring resonances as well as resonances of other isotopes in the mixture, has been developed.

Calculations have been made for both U^{235}:U^{238} and Pu^{239}:U^{238} systems with various enrichment ratios and probable scattering cross sections. With the general expression and a slight modification of the existing code, it is possible to study the following cases separately: (1) fissile and fertile materials are homogeneously mixed; and (2) fissile and fertile materials are physically separated so that only the former is heated.

In the first case, a significant reduction in the Doppler broadening is observed in all intermediate energy regions of interest. The effect is particularly marked for the U^{235}:U^{238} system. In fact, the Doppler broadening of U^{235} resonances changes its sign between 0.5-15 keV due to the resonance overlapping. In the second case, however, a relatively small reduction in the Doppler broadening is observed mainly due to the overlap of neighboring resonances. The effect from the cold fertile isotope is small.

3. Orthonormal Expansion of Neutron Spectra with Foil-activation Measurements

A computer program for investigating the orthonormal expansion method has been developed.[5] Preliminary results have been obtained for a test problem in which an attempt was made to fit a specific neutron spectrum

---

[5]Reactor Development Program Progress Report for October 1963, ANL-6801, p. 41.

from a given set of activation measurements. A modified form of the Watt fission spectrum[6] was selected for this test:

$$\phi(\epsilon) = a\epsilon^{-b\epsilon} \sinh(c\,\epsilon)^{1/2}. \tag{1}$$

The constants a, b, and c of Eq. (1) are

$$a = 0.453; \quad b = 1.035; \quad c = 2.29. \tag{2}$$

Thereby $\phi(\epsilon)$ satisfies the normalization condition

$$\int_0^\infty \phi(\epsilon)\, d\epsilon = 1. \tag{3}$$

The ten activation cross sections presented in Table VIII were utilized in this test problem. By use of the cross sections for these reactions together with the spectrum given in Eq. (1), theoretical activations have been determined by numerical integration. With these activations, one can obtain approximations of the spectrum in the form

$$H_n(\epsilon) = \sum_{i=1}^{n} \gamma_i U_i(\epsilon). \tag{4}$$

In this particular investigation, the orthonormal set of functions $\{U_i(\epsilon)\}$ were generated by the Gram-Schmidt process. Hence, it is appropriate to call this particular orthonormal approximation, the Gram-Schmidt method.

Table VIII. Activation Reactions

n		n	
1	$Li^6(n,\alpha)$	6	$S^{32}(n,p)$
2	$Al^{27}(n,\alpha)$	7	$K^{39}(n,p)$
3	$Al^{27}(n,p)$	8	$In^{115}(n,n')$
4	$Si^{28}(n,p)$	9	$Np^{237}(n,f)$
5	$P^{31}(n,p)$	10	$U^{238}(n,f)$

As a measure of the error associated with a given approximation $H_n(\epsilon)$, it is convenient to introduce the residual E_n, defined by

$$E_n = \int_0^\infty |H_n(\epsilon) - \phi(\epsilon)|\, d\epsilon. \tag{5}$$

---

[6] L. Cranberg et al., Fission Neutron Spectrum of U^{235}, Phys. Rev. 103, 662 (1956).

In view of the normalization condition, Eq. (3), one may also call E_n the relative error of the approximation.

Figure 6 presents the relative error E_n as a function of n, obtained from the Gram-Schmidt method for this test problem. Extrapolation indicates a limiting accuracy (i.e., $n \to \infty$) of roughly 25% is available with this particular method. A comparison of the approximation $H_9(\epsilon)$ with the original spectrum $\phi(\epsilon)$ is given in Figure 7.

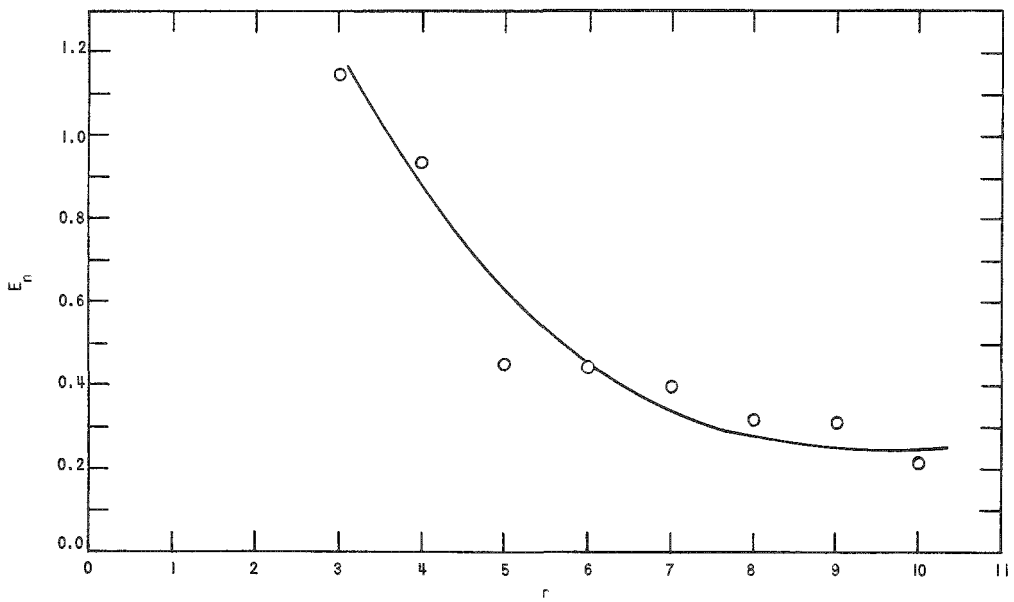

Figure 6. The Relative Error, E_n, as a Function of n

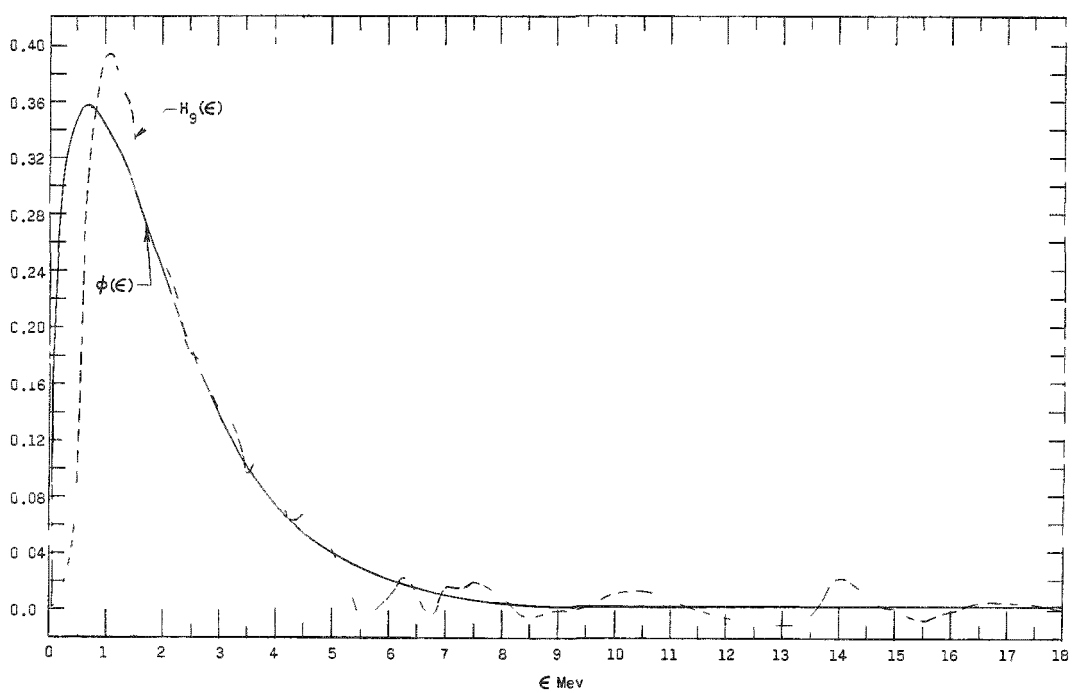

Figure 7. A Comparison of $H_9(\epsilon)$ and $\phi\epsilon$ for the Gram-Schmidt Method

It should be stressed that the accuracy presented above is definitely the best that can be attained for the Gram-Schmidt method, since experimental error has not been included in the analysis. Further work will include an analysis of the effects introduced by experimental error. The source of experimental error which arises from uncertainties in the cross sections that are employed, may significantly affect the end results. The computer program will be extended in an effort to investigate these effects.

4. Excursion Analyses for Fast Reactors

A series of AX-I calculations were initiated to compare the energy release from a homogeneous core with that from a power-flattened core with a relatively long (~15 μsec) initial prompt neutron lifetime. The systems are moderator reflected. The relatively flat power distribution in the core was obtained by varying the ratio of fuel to strongly absorbing diluent as a function of radius. Actually, the ratio is held constant for radial shells, thus giving a "chopped" but relatively constant overall power distribution. Table IX summarizes some significant excursion parameters. It is to be noted that the "autocatalytic" behavior of these excursions (see Monthly Progress Report for July 1963, ANL-6764, p. 40) appears to be somewhat aggravated by a system with a relatively flat power distribution. The prompt neutron lifetime of the power-flattened systems is usually somewhat shorter (by ~5 μsec) than the homogeneous core system. Similar comparative analyses are being initiated for systems with shorter (<0.5 μsec) prompt neutron lifetimes.

Table IX. Comparative AX-I Analyses
(300-liter, Moderator-Reflected Cores)

Core Type	Period (μsec)		Peak Pressure (megabars)	Time of Peak Pressure (μsec)	Time (μsec) Period Becomes Negative	Energy Release (10^{16} erg)	
	Initial	Minimum				Kinetic	Total
Homogeneous	250	220	0.15	1092	1188	0.029	4.6
Flattened	345	263	0.16	1410	1467	0.10	8.2
Flattened	297	188	0.19	1206	1240	0.18	10.8
Flattened	168	129	0.26	894	901	0.54	15.5

C. Reactor Fuels Development

1. (Th,U) Phosphides

As part of a study of (Th,U) phosphides, thorium monophosphide was synthesized by the reaction of phosphine (PH_3) gas with finely divided thorium obtained from the hydride. The surfaces of the thorium chips used were cleaned in a 50% solution of HNO_3 containing some HF. Comminution of the thorium chips was somewhat more difficult than that of

uranium chips and generally required more hydriding cycles. Reaction with phosphine proceeded most smoothly at a temperature of 550°C to give a black powder. X-ray analysis revealed that Th_3P_4 was the major phase, with some ThP, ThO_2, and thorium hydride as minor phases. The material was calcined in vacuum at 1300°C to homogenize it and drive off excess phosphorus. Considerable outgassing occurred between 1150 and 1200°C, indicating that Th_3P_4, like U_3P_4, dissociates in vacuum in this temperature range. The calcined material was dark blue and yielded a very sharp X-ray powder pattern. The lattice constant of 5.83 Å corresponded to the literature value for the compound. In addition, the X-ray pattern showed only small amounts of ThO_2 contamination, corresponding to about 0.3% of oxygen.

ThP appears to be more resistant to oxidation than UP. DTA studies revealed that a minor oxidation exotherm occurred at about 550°C and a major one at 660°C. With UP two exotherms of about equal strength occurred at 450°C and 560°C. ThP also appeared to be more resistant to oxidation than ThS. The retardation of oxygen attack is probably a result of the formation of a coating of P_2O_5 on the grains. The properties of ThP will be studied, as well as those of ThP-UP solid solutions which will be prepared shortly.

2. Uranium Monocarbide

In connection with the method of preparing uranium monocarbide by the reaction of uranium halides with carbides in molten salt solvents, several experiments have been performed to determine whether uranium monocarbide is soluble in molten chloride systems of interest and whether the carbide reacts with the constituents of the salt. In preliminary tests in which uranium carbide was held in molten salt, there was no evidence of a measurable solubility of uranium carbide in either LiCl-KCl at 650°C or in LiCl-$MgCl_2$ at 600°C.

D. Reactor Materials Development

1. Irradiation Damage in SA212B Pressure Vessel Steel

a. Irradiations in EBWR. Five helium-filled capsules containing round multi-notch impact specimens and combination magnetic-sonic bars prepared from unstressed 4-in.-thick SA212B plate were examined for changes in properties after irradiation at temperature in the EBWR. The following table summarizes the history of the irradiation cycle of the steel.

Group No.	1	2	3
No. of Capsules	1	3	1
Location	Irradiation Thimble	Irradiation Thimble	Steam Dome
Thimble Irradiation Exposure, MW/hr	8395	75,755	0
Exposure, hr	530	2298	2298
Core	48-in.-diameter, 20-MW Spiked Core	48-in.-diameter, 20-MW, + 60-in.-diameter, 100-MW	Control Specimens for Thermal Effects

Some capsules were irradiated in a normal irradiation thimble while others were irradiated in a thimble surrounded by 2 w/o boron stainless steel. There were no differences in properties between the samples irradiated in the bare thimble and those samples protected by boron steel.

The impact transition temperature data obtained supported the following conclusions:

(1) Control samples (outside the irradiation damage region) showed a moderate thermal embrittlement; the fracture-transition temperature curve was elevated 20-25°F at constant fracture energy.

(2) Irradiation effects following 530-hr exposure were either absent or masked by the metallurgical embrittlement at the 488°F reactor temperature.

(3) The additional irradiation during the 100-MW reactor operations simultaneously shifted the transition temperature upward by 100-125°F and reduced the fracture energy by about 25%.

(4) No significant differences in resistance to impact were found in the steel specimens irradiated in either the "bare" or "shielded" thimbles.

Neither the dc coercive force and permeability nor the 60-cps ac magnetic properties (which included saturation induction, coercive force, permeability, remanence, and losses) were affected by the irradiation. Postirradiation thermal heat treatments at temperatures as high as 1500°F affected the dc coercive force slightly. Complementary studies with cold-rolled steel stock showed that the changes of magnetic properties following thermal annealing (to 1500°F) were much greater and totally unlike that of the irradiated SA212B steel.

Resonant and third-harmonic frequency measurements for the transverse vibrational mode revealed that irradiation did not affect these characteristics. Accompanying measurements of the logarithmic decrement were also found to be unchanged.

b. MTR-ANL-26 Irradiation of SA212B EBWR Head Steel. A few multi-notch irradiated impact bars cut from unirradiated SA212B steel used in the fabrication of the lower head of EBWR were also examined for changes of magnetic properties. This steel, an entirely different and historically earlier heat, was irradiated to dosages two orders of magnitude greater than that described in a. above. Both the as-irradiated and the subsequently thermally annealed bars, annealed at 1200 and 1500°F for holding times as long as 2 hr at temperature, were found to be magnetically like the unirradiated material. There were no changes in the dc coercive force and in the 60-cps ac family of minor hysteresis plots from which saturation induction, remanence, ac coercive force, permeability, and hysteresis losses were derived.

c. EBWR Vessel Material in Use in EBWR. Both the dc and 60-cps ac magnetic properties of the operating EBWR pressure vessel material were very similar to unstressed head plate material. Resonant and third-harmonic frequencies of standard 0.204-in.-dia by $3\frac{3}{4}$-in.-long bars were unchanged by fabrication or by the accumulated operational history at temperature. Internal resistance, as measured by the logarithmic decrement, was increased by a factor of two by fabrication and/or service history at temperature. The observed rise in the transition temperature of SA212B bars held at temperature in the EBWR irradiations are probably related to the increase in internal friction.

The measurements of resonant and harmonic frequencies of EBWR vessel steel before and after irradiation, and of vessel material with a known operational history are significant in fracture mechanics analyses. Young's modulus of elasticity was unchanged. Increases in internal friction are also significant as this relates to the stress wave energy conversion mechanism.

Similar measurements of a limited number of bars of SA212B material from the SL-1 pressure vessel were completed. The data are being analyzed.

E. Reactor Components Development

1. Electric Master-Slave Manipulator Mark E4

The slave arm of this manipulator is connected to the master arm with only a multiconductor electrical cable and can, therefore, work throughout a large volume. The reflection of load forces to the master

arm and the low inertias, frictions, etc., enable the operator to utilize his position and kinesthetic senses to perform complex operations. The slave arm can be positioned by a support system on the ceiling or walls of the cell, or by a vehicle on the floor. The load capacity of this manipulator is 50 lb, the same as that of the Electric Master-Slave Manipulator Model 3. However, there are a number of improvements; improved dependability, ability to be remotely repaired, better reach capabilities, and a lower reproduction cost. The electrical system of this manipulator will permit master and slave to be separated by up to 2,000 ft.

The improved reach is achieved by providing a telescopic lower arm along with a counterweight system which allows the upper arm to rotate 360° about its axis. Thus, the arm can approach and reach the work in most all directions.

The first version of the slave arm is being designed so that it can be completely and remotely repaired by a pair of similar arms equipped with adequate tools. Subassemblies are designed so that they can be remotely removed, and the larger of these can then be remotely repaired. Individual parts and small subassemblies are designed so that they can be remotely replaced.

Each of the seven motions of the slave arm has an electrically operated brake. These brakes can be set or released by the operator, or will be set automatically by the fail-safe circuit in case of electrical malfunction.

The position difference between the master and slave arm motions is measured by low-impedance phase shifters instead of the conventional synchro system. This system reduces the number of conductors needed in the electrical cable connecting master and slave arms, and provides a reasonably good signal for operating the fail-safe circuit.

The maximum force capabilities of the slave arm in any direction is 50 lb, and the maximum force capabilities in the master arm is 17 lb. The force at the master arm can be selected to be equal to the force at the slave arm from 0 to 17 lb, or the slave arm can be operated from 0 to 50 lb with the feedback force of only $\frac{1}{3}$ of the load at the slave arm. The forces on the master arm are limited to avoid injuring the operator in case of electrical malfunction and to decrease the work the operator must do in handling heavy loads.

The design layout of the mechanical components of the remotely repairable slave arm is approximately 75% complete, and about 45% of the detail drawings have been finished. The design and layout of the mechanical components for the master arm is approximately 40% completed. Approximately 10% of the details have been drawn. Manufacturing of the detail

parts and subassemblies for both the master and slave arms has been started. A prototype of the servo system for one motion has been built and tested. Most of the electrical components for two complete manipulators are on hand.

F. Heat Engineering

1. Boiling Sodium Heat Transfer Facility

Preparations for testing the 150-kW power supply are continuing. To avoid the expense of a completely new (and expendable) bus bar and current transformer installation, the power supply will be tested at about 4000 Amp instead of the maximum rated value of 10,000 Amp. A water-cooled load for this use has been designed and is being fabricated. The power-supply installation for this equipment has been completed, checked out, and accepted. A precision wattmeter, voltmeter and ammeter, and a current transformer have been obtained for this test. Some preliminary design work has been accomplished on the vacuum chamber work platform, columbium alloy pipe fittings, and sodium dump tank seals.

2. Two-phase Critical Flow

Thirty blow-down tests have been carried out at the present time. Two sharp-edged orifices, $\frac{1}{4}$ in. and $\frac{1}{2}$ in. in ID, and tubes with length to diameter ratios of 40, 32, 24, 16, 12, 8, and 6 have been tested. Initial conditions varied from 200 to 1800 psia, and with saturated or slight subcooled conditions prevailing at the time of blow down.

The major conclusions from the orifice tests are:

a. The fluid remains completely metastable.

b. The obtained flow rates can be calculated by the orifice equation:

$$G = A(0.611)\sqrt{2g\rho\Delta P}\,.$$

The data obtained with the various tubes have not been completely analyzed, but the following observations have been made. The upper limit of exit qualities is 10-15%, and critical exit pressures up to 1000 psia were obtained. The critical pressure ratio remains approximately constant during blow-down, seems independent of initial pressure, and varies only from 0.55 to 0.6 as the L/D ratio varies from 40 to 8.

At an L/D ratio of 6, these criteria seem to break down. The critical pressure ratio decreases sharply at L/D = 6 and is dependent on initial conditions. For the tube tests with L/D ratio of 8 and 6, significant

oscillations of the pressure profile in the test tubes were observed. The magnitudes of the oscillations were larger for L/D ratio of 6 and increased for decreasing initial pressure.

The establishment of these oscillatory flows is likely due to increased metastability for decreasing L/D ratios.

Preparations are now being made for studying discharge rates in tubes of L/D ratios from 6 to approaching 0. Design criteria will hopefully be derived that can predict the discharge rate of saturated water for any geometry given.

Data are being taken in such a way that if initial conditions (pressure and temperature) and geometry are given, flow discharges can readily be estimated. The limits at which various existing models can be utilized will be critically examined.

G. Chemical Separations

1. Chemistry of Liquid Metals

a. Cerium-Zinc System. The partial pressure of zinc over two-phase mixtures of cerium-zinc intermetallic compounds has been measured as a function of temperature by the Knudsen effusion cell method. The two-phase mixtures studied were $CeZn$-$CeZn_2$, $CeZn_2$-$CeZn_3$, $CeZn_3$-$CeZn_{3.5}$, $CeZn_{3.5}$-$CeZn_{4.3}$, $CeZn_{4.3}$-$CeZn_{5.25}$, $CeZn_{5.25}$-$CeZn_7$, $CeZn_7$-$CeZn_{8.5}$, and $CeZn_{8.5}$-$CeZn_{11}$. The results are in generally good agreement with those reported by Chiotti and associates,[7] who used the dew point method.

b. Lanthanum-Cadmium Galvanic Cell Studies. The thermodynamic functions of the lanthanum-cadmium system are being evaluated by means of a galvanic cell. Studies of the rare earth-cadmium systems, together with parallel studies of actinide metal-cadmium systems, are of utility in the design of practical processes for the separation of thorium, uranium, and plutonium from rare earth elements.

A new cell of the form $La/LaCl_3$, KCl-LiCl (eutectic)/La-Cd (two-phase alloy) has been assembled, and the emf of the cell has been measured as a function of temperature. The free energy of formation of $LaCd_{11}$ may be represented by the equation

$$\Delta G_f^\circ \text{ (cal/mole)} = -72{,}890 + 44.39\,T$$

over the temperature range from 400 to 530°C.

---

[7] Chiotti et al., Annual Summary Report, Ames Laboratory, IS-700, 1962-1963, p. M-23.

c. Distillation of Liquid Metals. The effectiveness of a de-entrainment device which was installed in the large unit for distillation of cadmium has been determined in five runs in which lead was added to the cadmium charges as a nonvolatile component. Entrainment of liquid as measured by the carryover of lead during distillation was lower by as much as a factor of seven than in the absence of the device, but still ranged from 0.9 to 2.3 percent. This general level of entrainment is higher than is desirable for an evaporation or retorting operation in which uranium or plutonium is separated from a metal solvent such a cadmium, zinc, or magnesium. Nevertheless, a de-entrainment device can be used in conjunction with an appropriate distillation and retorting technique to reduce entrainment to satisfactory levels. For an evaporation operation, entrainment can be minimized by providing reflux within the crucible. For a retorting operation, the problem can be circumvented by keeping the uranium in a precipitated form during retorting.

Studies of the vaporization of mercury from a 1-in.-dia resistance-heated liquid pool without the formation of bubbles (nonturbulent vaporization) were continued. During the month, the vapor-phase pressure was measured closer to the vaporizing surface than in previous runs. Also, vertical traverses into the mercury pool were made at several radial distances from the pool centerline with a new thermocouple having a 10-mil exposed hot junction. Based on the pressure existing just above the surface of the pool, a value of 22°C was obtained for the surface superheat through the mercury surface at a vaporization rate of 115,000 Btu/(hr)(sq ft). The results of temperature traverses taken at different radial distances from the pool centerline showed that in the shallow surface layer (see Progress Report for October 1963, ANL-6801, p. 57) temperature gradients were 165°C/in. at the pool centerline and 121°C/in. near the edge of the pool.

2. Fluidization and Volatility Separation Processes

a. Recovery of Uranium from Low-enrichment Ceramic Fuels

(i) Laboratory-scale Facility for Fluid-bed Fluorinations. Work is essentially completed on the installation of a second laboratory-scale facility for carrying out fluid-bed fluorination process studies in a 2-in.-diameter reactor. In this facility, studies of the fluorination of mixtures of U_3O_8 and plutonium dioxide will be continued (see Progress Report for November 1963, ANL-6808, p. 53). This facility will provide greater flexibility for performing laboratory experiments than was possible in the facility with the $1\frac{1}{2}$-in.-diameter fluid-bed fluorinator reactor (see Progress Reports for June 1963 and November 1963, ANL-6749, p. 43, and ANL-6808, p. 53). Both facilities will be used for carrying out programmatic research of process studies. Equipment has also been installed in the new facility for carrying out the oxidation or hydrofluorination

of large amounts (up to one kilogram) of UO_2-PuO_2 solid solution powders or pellets and for the preparation of homogeneous powder mixtures. Shakedown runs with U_3O_8 to test operationally the fluorinator reactor and its associated equipment are expected to begin in early 1964.

(ii) Plutonium Pilot Plant Facility. Work on the installation of an engineering-scale plutonium-handling facility is continuing (see Progress Report for December 1962, ANL-6672, p. 37). The facility, which consists of two large alpha-containment gloveboxes of a modular type, will be used to study the various steps of the fluid-bed fluoride volatility process for the recovery of uranium and plutonium from plutonium-uranium oxide fuels. The fluorination step of the process will be studied initially. Equipment and accessories needed for this study have been installed. The installation of process piping is essentially completed. Testing of process components and instrumentation is under way. Testing was carried out of the bag-out procedure for vertically removing or inserting large equipment items through the 30-in.-diameter port atop each module of the alpha box. The test results were satisfactory and indicated that no difficulties should be encountered in this bag-out procedure.

b. Recovery of Uranium from Highly Enriched Uranium-Alloy Fuels by Chlorination and Fluorination Steps. An additional shakedown run has been completed in the pilot plant facility installed to demonstrate the recovery of uranium from highly enriched uranium-alloy fuels by means of the fluid-bed fluoride volatility process (see Progress Report for November 1963, ANL-6808, p. 57). In this run, a multiplate, welded subassembly which was fabricated from aluminum only was charged to the fluid-bed reactor. Since the subassembly did not contain uranium, only the hydrochlorination and hydrofluorination reaction steps were carried out. In future experiments with subassemblies containing uranium, the fluorination step will be included in the reaction sequence. During the hydrochlorination step, the fluid-bed pyrohydrolysis reactor was in operation to convert the volatile aluminum trichloride (which represents a waste stream) to a solid oxide.

The objectives of this run were to determine the effect of the following on the rate of the hydrochlorination reaction: (1) hydrogen chloride input rate, (2) surface area (number of plates) of the fuel charge, and (3) the reactor bed temperature.

The charge consisted of a 14-plate aluminum subassembly which was $2\frac{1}{2}$ in. by $3\frac{1}{8}$ in. by 48 in. long and weighed 12.1 kg. The reaction bed contained 40 kg (static bed depth of 50 in.) of -28 +100 mesh alumina;* the packed-bed filter contained 9 kg (bed depth of $6\frac{1}{4}$ in.) of

*Tabular type T-61 sintered grain alumina, a product of Aluminum Company of America.

-14 +28 mesh alumina. The starting bed material for the fluid-bed pyrohydrolyser was 21.5 kg of aluminum oxide (+100 mesh) remaining from the pyrohydrolysis of aluminum trichloride vapor in a previous run.

The hydrochlorination step was performed over a period of 7.9 hr at reaction bed temperatures which were varied between 320°C and 410°C. In this step, the hydrogen chloride concentration was increased stepwise, as follows: 55 v/o HCl in nitrogen for the initial 15-min feeding period; 65 v/o HCl in nitrogen for the second 15-min feeding period; and 79 v/o HCl in nitrogen for the remainder of the hydrochlorination period. The hydrofluorination step (about 20 v/o HF in nitrogen) was conducted at a fluid-bed temperature of 325°C over a period of 1.3 hr. The packed-bed filter and the fluid-bed pyrohydrolyser were operated at bed temperatures of 375°C and 320°C, respectively.

In general, operational performance was satisfactory. The fuel charge was completely reacted in the hydrochlorination time indicated above. A comparison of the preliminary results from this run with the results of a previous run (see Progress Report for November 1963, ANL-6808, p. 57) in which a 17-plate aluminum-only subassembly ($2\frac{1}{2}$ in. wide by 48 in. long) was charged to the reactor indicates that the hydrochlorination reaction rate increases with increasing hydrogen chloride feed rate and that the utilization efficiency for HCl appears to be dependent on the surface area available (number of plates) for reaction. In the current run, during the first 80% of the hydrochlorination reaction period (for the existing flow rates), increasing the reactor bed temperature from 320°C to 410°C (in two steps) had no noticeable effect on reaction rate or HCl utilization efficiency. During this period, the reaction rate was essentially constant at 1.7 kg aluminum/hr, and the HCl utilization efficiency was 60%. The overall reaction rate and HCl utilization efficiency for the run were 1.53 kg aluminum/hr and 50.5%, respectively. A maximum temperature of 465°C was observed in the channels between the aluminum plates of the subassembly during the hydrochlorination. Since this temperature is well below the melting point of aluminum (660°C), an increase in the reaction rate can probably be achieved without exceeding practical operating temperature limits.

The aluminum chloride produced in the hydrochlorination was converted to the oxide in the fluid-bed pyrohydrolysis reactor. A major fraction (about 87%) of the aluminum oxide was found to be in the form of fines smaller than 100 mesh. However, the presence of these fines did not affect the operation of the pyrohydrolysis reactor.

c. Corrosion Tests of Nickel. Corrosion studies are being carried out in support of the fluid-bed fluoride volatility program. The suitability of nickel as a material of construction in these processes is being

investigated. Sample specimens of nickel-200* (99.5% nickel) were prepared for testing: $\frac{1}{4}$-in.- and $\frac{1}{16}$-in.-thick plate (nonwelded); $\frac{3}{16}$-in.-thick plate welded** with either nickel-200 filler metal or nickel filler metal 61.† Both types of samples were inserted in heated furnace tubes and exposed to the following environments: (1) continuous flow of 50 v/o fluorine in nitrogen at 500°C, (2) alternating (each 24 hr) streams at 450°C of 50 v/o hydrogen chloride or 50 v/o fluorine in nitrogen, and (3) alternating (each 24 hr) streams at 500°C of 50 v/o oxygen or 50 v/o fluorine in nitrogen

At the end of 240 hr of exposure, the following preliminary results of corrosion rates for the nonwelded and welded samples were observed. In general, for the nonwelded plate specimens, low average penetrations (based on weight-loss data) were noted. The results were as follows: in environment (1), about 1 mil/yr; in environment (2), about 2 mils/yr; and, in environment (3), about 2 mils/yr Metallographic examination of these specimens for intergranular attack is in progress.

For the welded specimens, corrosive attack upon the nickel weld deposit varied considerably and depended upon the type of weld filler metal used. The corrosive attack on nickel weld deposits made with filler metal 61 was considerably higher than those weld deposits made with nickel-200 filler metal. However, at the root of the weld, where considerable dilution of the filler metal 61 with the parent metal (nickel) occurred during the first welding pass, the rate of corrosive attack was considerably less Titanium oxyfluoride ($TiOF_2$) has been identified by X-ray diffraction analysis as a major component in condensed solids found in the exhaust line of a test furnace after mixtures of oxygen or fluorine in nitrogen had been passed through the furnace. This identification of $TiOF_2$ would also tend to verify the preferential attack of nickel weld deposit made with filler metal 61.

H. Plutonium Recycle Program

Control rod worth calculations (see Progress Report for November 1963, ANL-6808, p 60) have been made for plutonium zone burnups of 0.003 and 0.006. At 0.003 burnup, the nine-rod worth decreased from the zero burnup value of about 17% to about 15%, and at 0.006 burnup the nine rods are worth somewhat over 14%. The central rod worth with the other eight rods in dropped from an initial value of about 4.5% to about 0.6% at 0.003 burnup and to about 0.2% at 0.006 burnup. At the same time

*Nickel-200 (formerly designated as "A" nickel) is a commercially pure, wrought nickel product and has the following nominal composition (in percent): Ni, 99.5; C, 0.06; Mn, 0.25; Fe, 0.15; S, 0 005; Si, 0.05; and Cu, 0.05.

**Welded by the inert gas tungsten arc process.

†A product of the International Nickel Co., Inc. Nickel filler metal 61 has the following nominal composition (in percent): Ni, 93.0; Ti, 2.00-3.50; C, 0.15; Mn, 1.0; Fe, 1.0; S, 0.01; Si, 0 75; Cu, 0 25; Al, 1.50; and other, 0.50.

the off-center corner rods increased in worth from about 6% initially to about 7.5% at 0.006 burnup. The worth of the off-center, non-corner rods changed very little at 0.006 burnup as compared with zero burnup. The changing rod worth results in a cold shutdown reactivity margin of about 2% initially, about 0.5% at 0.003 burnup, and essentially zero at 0.006 burnup.

Reloading of the shim at 0.006 burnup has little influence on the rod worth. Experience gained during the course of the irradiation may indicate that the reactivity and rod worths vary with burnup in such a way that reloading of the shim as originally planned is not indicated.

Calculations have been performed with the 20-GRAND code and a correct four-group scattering matrix. Comparison of these results with PDQ calculations, which use an approximate scattering matrix, has verified the accuracy of the PDQ results for rod worth, which include corrections obtained from the RP-122 code.

The PDQ code has been used to obtain the worth of a central plutonium fuel element and of a central first shim row element for the cold system at zero burnup. These are worth respectively about 0.6% and 0.3% relative to water.

The boric acid worth has been obtained for the cold system at zero burnup. An addition of 1 gm/gal of water results in a reactivity reduction of about 1%. The void coefficient of reactivity for the cold zero burnup system is about -0.1 for $\delta k/\delta V$ and is essentially independent of boric acid content up to 10 gm/gal of water.

A CYCLE 2 calculation has been run for the system having the void distribution corresponding to that expected at 0.006 burnup to examine the influence of voids on the isotopic variation in the plutonium zone. Comparison of the resulting isotopic concentrations with the values obtained using the void distribution corresponding to the zero burnup configuration reveal changes of less than 2%. This difference is of course only an estimate since the void distribution changes continuously as the burnup proceeds whereas the CYCLE calculations holds the voids constant with burnup.

IV. ADVANCED SYSTEMS RESEARCH AND DEVELOPMENT

A. Argonne Advanced Research Reactor (AARR)

1. Critical Experiment

A contract for the procurement of fuel foils for the AARR critical experiment has been signed. The contract provides for an initial 300 foils of bare (unclad) uranium metal to be delivered in April 1964, and contains an option for the procurement of an additional 1018 foils at a stated fixed price. This option, exercisable within 3 months, will be taken up after additional FY 1964 research and development funds have been obtained for AARR.

Assembly of beryllium reflector, as well as the cleaning of the dump tanks, pipes, and the reactor vessel, for the critical experiment are progressing. Much of the electronic equipment is now in acceptable condition for startup. Interaction between electrical circuits still is so strong, however, that spurious scrams occur not only in the AARR console but also in the adjacent ZPR-VII facility. Noise-suppression techniques are expected to reduce this problem significantly Channels III, IV, V, and VI operate quite satisfactorily through their operating ranges with signals derived from ZPR-VII operation Channels I and II are operable but troublesome, being particularly sensitive to switching transients when interlock relays and other switches operate.

A PERT study of the AARR critical experiment program predicts a duration of almost 2 years, beginning with initial criticality in July 1964. This is longer than had previously been anticipated. Some of the methods under evaluation to shorten the duration are:

a. reduction of the time required for each experimental run by reducing the number of control rods to be inserted and withdrawn each time, reduction of the volume of water drained rapidly upon shutdown, and increasing the capacity of the filling pump;

b. incorporation of automated techniques for data processing;

c. assignment of additional personnel.

d. elimination or curtailment of certain experiments, or postponement so that results can be incorporated into later AARR cores, but not the first core.

2. Reactor Control

Analog computations of the transient behavior of the AARR (40-40) core with reference design conditions imposed for 240-MW operation have been completed. The core model used did not include a treatment of hot

channels; hence, coolant boiling was not incurred except for large changes from the steady state. Preliminary examination of the results indicates the following:

a. The core is inherently very stable.

b. To avoid bulk boiling in the core during flow coastdown, a power setback must be effected within one second after loss of primary pumping power.

c. The core responds safely to substantial ramp rates in inlet water temperature

d. A large loss of system pressure results in power reduction due to feedback reactivity arising from steam generation. Temperatures remain normal but a small power oscillation is observed.

e. With respect to short-term responses to step-input reactivity, power excursions are limited such that no bulk boiling occurs for insertions up to $0.75. Maximum fuel temperatures approach the melting point for a step insertion of reactivity of $1 05

f. With respect to long-term responses to step-input reactivity, bulk boiling is incurred for an insertion of $0.75, i.e., after a short period of bulk boiling during the initial power pulse, water temperatures drop below saturation and then rise to the boiling point approximately 4 sec after application of the step. Maximum fuel temperatures reach the melting point only for those cases wherein the melting point is exceeded in the short-term response.

3. Heat Transfer

The high heat fluxes and local boiling conditions which will be encountered in high-power operation of AARR have necessitated experimental heat transfer studies The large D-11 heat transfer loop facility will be used for this test program.

A modified technique for fabricating test sections for these experiments has been developed and is expected to result in substantial reductions in test-section cost. Design has been completed of an initial test section which is intended primarily to check the feasibility of the modified fabrication method and to serve in the loop during equipment and instrumentation checkout. The flow channel in this section is 1.25 in. wide, 0.040 in. thick, and 22 in. long, with an 18-in. heating length, and is designed to provide a uniform heat flux along the length. The section is being fabricated of nickel "A."

4. Shielding

Studies have disclosed the need for shielding of coolant pipes in the control rod drive room and the spent-fuel-transfer system in the fuel-transfer cart drive room.

The coolant pipe shielding is needed because of several sources, the most intense of which is the contaminated coolant which would result from a fuel meltdown accident. While the damaged core remains in the circulating coolant system, the possibilities for coolant cleanup are limited. Access to the control rod drive room is required prior to core removal.

Shielding in the fuel-transfer cart drive room is needed in the event the cart becomes inoperable while transferring spent fuel. A second shield function is to limit flash-type radiation through the pipe tunnel.

Shielding considerations suggest interchanging the degasifier and deionizer cubicles, and revising the entrance to the auxiliary coolant systems cubicle.

B. Magnetohydrodynamics (MHD)

1. MHD Power Generation - Jet Pump Cycle

The source of the high pressure drop reported in the previous report (ANL-6808, p. 64) was traced to a clogged filter located before the flowmeter. This clogged filter was cleaned and pressure drop tests continued. Subsequent tests with the small-diameter constrictions showed that the pressure drop increased parabolically as higher flow rates were approached. This indicates severe limitations imposed on hydraulic losses at higher velocities for this particular configuration.

Additional tests were tried with the new nozzle and combiner design. The output rate for the steam from the nozzle was found to be so high that pumping could not be established without steam blocking of the channel. An attempt was made to locate a condition of dynamic stability in operation. This was tried by, first, establishment of water flow by means of a centrifugal pump, followed with simultaneous operation of the jet pump. Next, the centrifugal pump was cut out of the circuit by opening a bypass valve and shutting down the pump. Up to the present, a condition of good stability has not been found.

C. Direct Conversion

1. Sodium Cell - Thermionic Conversion Experiments

The experimental apparatus previously used to investigate thermionic energy conversion with cesium and potassium plasmas has been tested with a sodium plasma. The equipment, described in previous reports, is equipped with a tantalum emitter and molybdenum collector.

An X-Y recorder and VTVM were used to measure the output data. The cell was operated with the collector at -6 to +8 V with respect to the emitter, which was grounded.*

The following quantities were measured:

(1) dc voltage current characteristics;

(2) dc power output;

(3) sodium ion current;

(4) rf output and rms voltages.

The following parameters were varied:

(1) the emitter-collector distance;

(2) the emitter temperature;

(3) the sodium pressure and density.

Figure 8 and Table X show the results of a typical experiment.

A spectrochemical analysis of the sodium showed less than 300 ppm of potassium present and much less of the other alkali metals. These impurities are not believed to have any significant effect on the performance of the cell. However, sodium of still higher purity has been ordered and will be tested.

With a value of 5.12 V as the ionization voltage for sodium, the amount of ionization, as determined by the Saha-Langmuir equation, will be small. Assuming the work function is 4.2 V for the bare tantalum emitter, α(the ratio of ions to ions plus neutral atoms) will vary from about

---

*The maximum dc power occurs always at the knee of the characteristics. The maximum rf output is situated close to zero volt dc. The frequency and rms voltage of the rf is shown at +1, zero, and -1 V dc applied to the collector.

2.4×10^{-3} with an emitter temperature of 2000°K to 8.27×10^{-3} for an emitter temperature of 2600°K. The required sodium pressure and density must, therefore, be about two orders of magnitude higher than that required for cesium or potassium to achieve space-charge neutralization. For densities of 5×10^{12} to 1.6×10^{14} atoms/cc the calculated and experimental values agree quite well. For lower sodium densities the measured value of α appeared to be higher than that given by the Saha-Langmuir equation. This discrepancy may possibly be due to the effect of step ionization occurring between the excited and the ionized state.

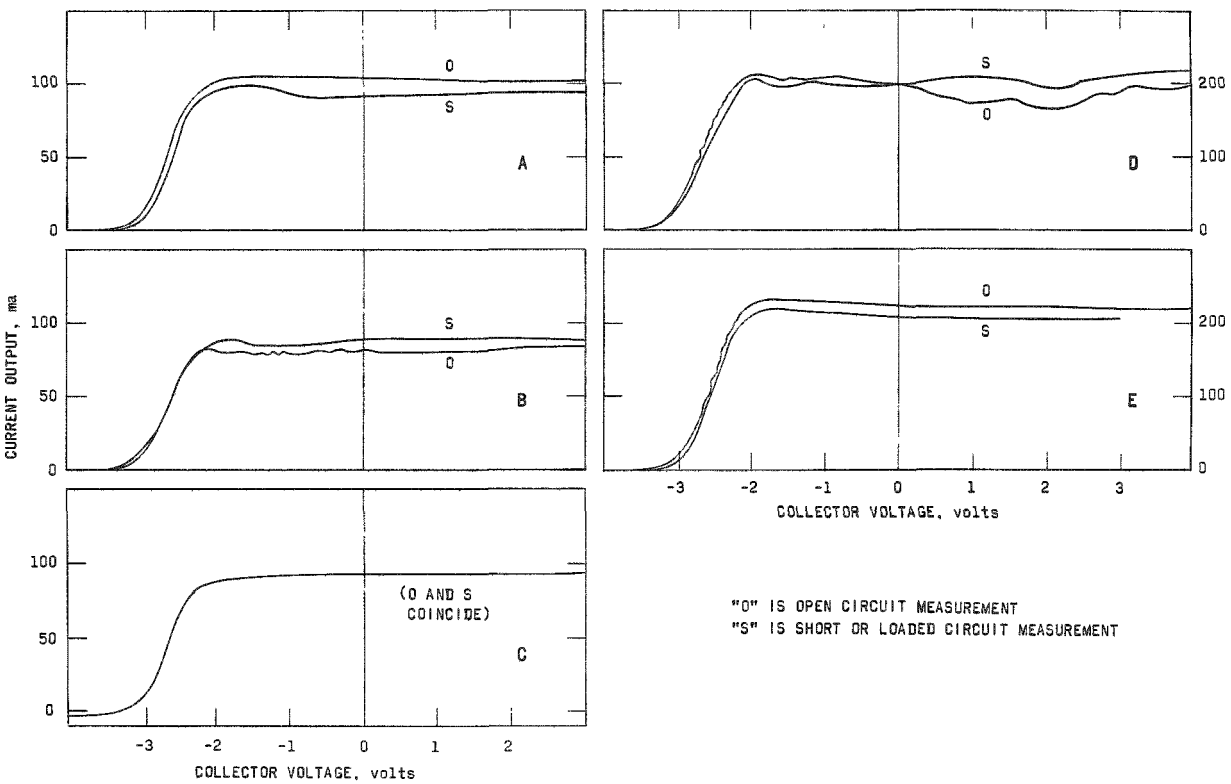

Fig. 8. Output Performance of a Thermionic Conversion Cell When a Sodium Plasma is Used to Neutralize the Space Charge.

Table X. Performance of a Thermionic Conversion Cell with a Sodium Plasma (at a Density of 1.6×10^{14} atoms/cc) to Neutralize the Space Charge

1	2	3	4	5	6	7	8	9	10	11	12
					Output Voltage and Frequency						
					Collector Voltage						
					+1		0		-1		
Graph No.	Emitter-Collector Distance, mm	Temp, Emitter °K	Ion Current, mA	Power Maxima, mW dc	Power Maxima, mW rf	kc	rms-V	kc	rms-V	kc	rms-V	J_E/J_i (Electron Current / Ion Current)
A	1	2275	2.5	210	-	450	0.95	?	0.4	120	0.6	44
B	2	2265	1.2	180	20	?	2.2	?	1.7	?	1.1	73
C	0.6	2265	3.0	190	-	520	1.0	510	0.3	220	0.2	30
D	2	2341	3.5	252	40	800	2.6	700	1.2	600	?	60
E	1	2341	3.5	260	-	?	0.6	?	0.5	?	0.5	65

2. Collector Work Function

The knee of the voltage-current characteristics for dry emitters is observed to occur at about -2.4 V. If the emitter work function is assumed to be 4.2 V, the collector work function will be 1.8 V. Comparison of these results with values found for cesium and potassium showed that the work function of the sodium-covered collector was only about 0.3 V higher than for cesium.

3. Excitation and Ionization

Some factors affecting the excitation and ionization of the sodium atoms were studied and measured as a function of a dc voltage applied to the collector. Starting with about +5 V on the collector, a sodium density of 2×10^{14} atoms/cc, and emitter temperatures of 2300-2600°C, an intense yellow glow was observed in the cell, and the current output reached a value of several amperes. As the applied voltage was decreased to zero, the yellow glow decreased in intensity as the current output fell.

4. Power Output and Voltage - Current Characteristics

Dc power outputs of several watts were obtained with an emitter temperature of 2600°K. At the higher emitter temperatures, the cell characteristics indicated a negative space charge was present in the cell. Rf oscillations were also observed similar to those reported for cesium and potassium plasmas. The rf power outputs reached about 10% of the dc power maximum.

D Regenerative EMF Cells

1. Bimetallic Cells

One of the bimetallic cells under consideration in the program for the development of a thermally regenerative emf cell is the lithium-bismuth cell (see Progress Report for November 1963 ANL-6808, p. 66). Experiments were carried out to determine the reason for the observed irreversible transfer of both lithium and bismuth metal from the anode and cathode molten metal electrodes. It is fairly well established that lithium metal shows a low but increasing solubility in the electrolyte with temperature. However, it was surprising to find that relatively large concentrations of bismuth were also found in the fused lithium salts (LiCl-LiF eutectic) which served as the cell electrolyte.

In the first experiment, the solubilities of pure bismuth in molten LiCl-LiF eutectic were determined over the temperature range from 873 to 1173°K. The solubilities were found to vary from 0.9×10^{-3} w/o at 873°K to 1.8×10^{-3} w/o at 1173°K. In the second experiment, the solubilities of a lithium-bismuth alloy (0.70 atom fraction lithium in

bismuth) in the same molten salt mixture were determined over the same temperature range The concentrations of bismuth in the molten salt mixture were about 0.31 w/o at 873°K and 3.74 w/o at 1173°K. The facts that the solubility of pure bismuth in the eutectic salt mixture is very small and that the differences between the solubilities of pure bismuth and those of the bismuth alloy are large (a factor of about 300 at 873°K and 820 at 1173°K) strongly indicate that the dissolution of bismuth from the lithium-bismuth alloy into the molten salt mixture cannot be due to the transfer of individual bismuth atoms from the alloy to the salt phase. Moreover, the amounts of lithium metal found in the salt phase over the temperature range studied gave an average lithium-to-bismuth ratio of 3.0 ± 1. These data strongly suggest that the dissolution of bismuth proceeds via the dissolution of the Li_3Bi compound This is thought to be the first observation of solubility of an intermetallic compound-type species in a fused salt

V. NUCLEAR SAFETY

A. Thermal Reactor Safety Studies

1. Metal Oxidation and Ignition Studies

a. Oxidation of Uranium-10 w/o Molybdenum Alloy. A uranium-10 w/o molybdenum alloy is being considered for use as core material in a critical assembly, "Super Kukla," at the Lawrence Radiation Laboratory. To aid in the evaluation of possible hazards that might be associated with the use of this alloy, short studies of its oxidation and ignition behavior have been undertaken. Alloy samples provided by the Lawrence Radiation Laboratory are being used in the studies

Bare samples, exposed to dry air (containing less than 5 ppm water) or wet air (air saturated with water at room temperature) were heated at a uniform rate of 10 degrees/min to about 775°C and were then held at this temperature. The oxidation behavior of the alloy was found to be the same in both environments No weight gains, as measured by a thermobalance, occurred below 350°C. At about 770°C, the oxidation rate was about 0.4 mg $O_2/(cm^2)(min)$ in both dry and wet air

A nickel-plated sample of the alloy showed negligible weight gain in wet air while being heated to about 760°C. Above this temperature the rate of oxidation increased rapidly, and self-heating of the sample to 945°C was observed The rate of the oxidation reaction was about 72 mg/(cm^2)(min) at 925°C. The nickel plating appeared to protect the alloy temporarily against oxidation, but once the reaction began, the plating appeared to have a deleterious effect as evidenced by the high rate of reaction.

b. Burning-curve Ignition Studies of Plutonium and Plutonium-containing Alloys. The effect of moisture on the ignition temperature of two samples of plutonium was determined by means of the burning-curve method [8] One sample was in the form of a 5-mm cube; the other was a 0.11-mm-thick foil. Both samples were exposed to air saturated with water at room temperature (water content of the air was greater than 20,000 ppm). Although the ignitions occurred in slightly shorter periods of time than those required for ignitions in dry air, the ignition temperatures in wet air for the two types of samples were essentially identical with the ignition temperatures of corresponding samples in dry air. A similar experiment with a plutonium-2 a/o aluminum alloy (5-mm cube) yielded similar results. The ignition temperatures of plutonium and the plutonium-aluminum alloy in dry and wet air are as follows:

---

[8] Chemical Engineering Division Summary Report April, May, June 1961, ANL-6379, p. 192.

Sample	Type of Sample	Ignition Temperature (°C)	
		Dry Air	Wet Air
Pu	5-mm cube	524	522
Pu	0.11-mm-thick foil	283	282
Pu-2 a/o Al	5-mm cube	585,590	569

Studies of the ignition temperatures of uranium-30 a/o plutonium ternary alloys by the burning curve method were continued (see Progress Report for November 1963 ANL-6808, p. 70) These studies are being undertaken in an effort to find an alloy of suitable composition for zero-power critical experiments. An alloy having an atomic ratio of U:Pu of about 2:1 is desired. Binary alloys having this composition, or one near it, have a tendency to crumble; as a result, work with these alloys presents excessive pyrophoricity hazards.

Two of the ternary alloys studied previously (see Progress Report for November 1963, ANL-6808, p 70) showed promising ignition characteristics in dry air. These alloys had uranium-to-plutonium ratios of about 2.1 with about 6 a/o molybdenum or iron added. In the present study, the effect of moisture in the air (air saturated with water at room temperature) on the ignition behavior of these two alloys was determined. The burning curve of the molybdenum alloy was essentially the same in wet air as in dry air However the effect of moisture on the iron-containing alloy was marked Whereas in dry air the iron alloy did not ignite when heated to 820°C and showed only moderate self-heating in the range from 300 to 450°C the alloy, in wet air started to undergo considerable self-heating and reaction at about 300°C which resulted in its ignition at about 480°C

c Isothermal Oxidation of Plutonium. Previous studies of the isothermal oxidation of plutonium (see Progress Report for March 1963 ANL-6705, p 63) have shown that the mechanism of the oxidation reaction changes between 300 and 400°C so that there is a minimum in the oxidation rate at about 420°C. It has been proposed that a second protective oxide film forms at temperatures above 420°C. This film is a diphasic oxide with an oxygen-to-plutonium ratio between 1 7 and 1.98.[9]

It was of interest to determine whether an oxide film formed at the higher temperatures (above 420°C) would afford protection during oxidations carried out at lower temperatures. By increasing the resistance

[9]Chickalla, T D , HW-74802 (1962).

of plutonium to room-temperature oxidation, pre-oxidation of plutonium above 420°C might find utility in preparing plutonium for storage.

A high-purity plutonium sample was oxidized with oxygen at 438°C until 11,000 μg O_2/cm^2 was consumed; the oxidation rate was 63.0 μg $O_2/(cm^2)(min)$. While the specimen was maintained in the oxygen atmosphere, the temperature was decreased to about 150°C in a series of steps, the linear oxidation rate being determined in each step. The results of the tests showed that the oxidation rates of the pre-oxidized sample were lowered by a factor of from 9 to 50.

d. Thermal Conductivity of Metal Powders. It is anticipated that the study of the effects of particle size, temperature, pressure, and degree of oxidation on the thermal conductivity of metal powders will lead to a better understanding of the mechanism of ignition of metal powders and may thereby lead to better preventive measures against accidental ignitions.

The method of study utilized a line source of heat. The powders were composed of spherical uranium particles. The thermal conductivity of uranium powders of three size ranges (-16 +20 mesh fraction, -70 +80 mesh fraction, and -230 +325 mesh fraction) were determined in nitrogen atmospheres at various pressures. The results, tabulated below, indicate that the conductivity increases with particle size and with pressure.

Mesh Size of Particles	Thermal Conductivity, cal/(cm)(sec)(°C) x 10^4 at Pressure (N_2)	
	10^{-2} mm	10^3 mm
-16 +20	1.6	9.8
-70 + 80	0.25	8.0
-230 +325	0.05	5 6

The thermal conductivity does not change with pressure at very low absolute pressures; in the region of very low pressures, conductivity is due to particle contact.

The effect of oxidation on the thermal conductivity of the powders was investigated. The conductivity of uranium powder was found to decrease with the extent of oxidation. At 1000 mm pressure and 24°C, the thermal conductivities of the -70 +80 mesh powder were 8.0 x 10^{-4}, 6.8 x 10^{-4}, and 6.4 x 10^{-4} cal/(cm)(sec)(°C) for unoxidized, 1.36% oxidized, and 2.3% oxidized powders, respectively.

The effect of temperature on the thermal conductivities of both unoxidized and partially (1.36%) oxidized powders was studied. At one atmosphere, the thermal conductivities of both types of powders were found to increase with temperature over the range from 24 to 280°C.

2. Metal-Water Reactions

a. Laser-beam Heating Applications. Research on the application of laser-beam heating to metal-water reactions was continued. The experimental procedure was modified, the main modification being the use of quartz optical flats in the reaction cells. With the modified procedure it has been possible to obtain uniform, reproducible melting of small (1 mm x 1 mm x 5-mil-thick) samples of zirconium foil. On melting, the foil samples are transformed to spherical particles with fairly uniform oxide layers.

Future development of the method involves the use of high-speed motion pictures to determine the growth rate of the steam-hydrogen film surrounding a particle. Development of a two-color pyrometer to trace the temperature-time behavior of the particle is continuing. These procedures, along with chemical and metallographic analyses of the total extent of reaction, will provide a relatively complete determination of the combined effects of heat transfer and chemical reaction of heated metal particles suddenly exposed to water. These results should provide a more rigorous basis for the practical analysis of reactor meltdown situations.

b. Studies in TREAT. Four experiments with 89.35 w/o zirconium-10.65 w/o uranium (93% enriched) alloy plates were completed in TREAT. Two of the runs were carried out in room-temperature water and two in water which was initially heated to 285°C (1000 psia saturated water pressure). The objective of these experiments was to obtain data on heat transfer from heated fuel plates to the water environment. This is to be accomplished by interpreting the temperature-time traces obtained by means of a high-speed oscillograph used during the experiments. The observed heating and cooling rates and heat transfer coefficients will be applied to computer analyses in order to obtain generalized information of wide applicability to practical situations. In addition, information on the extent of the metal-water reaction caused by each of the four excursions was obtained.

The alloy samples in room temperature water received 155 and 270 cal/g of nuclear energy. The energy input of 155 cal/g was just enough to raise the temperature of the sample to its melting temperature, whereas the energy input of 270 cal/g was sufficient to melt the sample completely. The extent of the metal-water reaction was 5.3% at the lower energy input and 6.3% at the higher energy input. The samples in heated water received 169 and 315 cal/g of nuclear energy, which resulted in metal-water reactions of 2.3% and 13.1%, respectively. For completely melted samples, the extent of the reaction in heated water is somewhat greater than in room temperature water. This is consistent with previous out-of-pile studies of the zirconium-water reaction.

The first meltdown in water of a pre-irradiated 20% enriched uranium-alloy fuel pin (93.5 w/o uranium-5 w/o zirconium-1.5 w/o niobium) was completed in TREAT; the pin had a burnup of 1.5% of the U^{235} and was cooled for 2 yr. The pin was subjected to a transient having an energy input of 270 cal/g in an 84-ms period. This energy input resulted in complete melting of the fuel pin, with extensive formation of particles. The extent of the metal-water reaction was 22.6%. Both the physical and chemical changes noted were similar to those noted in previous experiments with cold, clean fuel of the same type at a similar energy. The results of the test with pre-irradiated fuel indicate tentatively that the presence of fission products does not markedly influence the behavior of uranium fuel during meltdown in water.

B. Fast Reactor Safety Studies

1. Calculations of Transient Pressures

The computer code for calculating transient pressures and coolant expulsion from heated channels (see Reactor Development Monthly Progress Reports, ANL-6784, p. 68, September, 1963; and ANL-6801, p. 73, October, 1963) has been used to calculate a series of cases ranging from hypothetical accident conditions for small sodium loop experiments in TREAT to full-scale fast reactor geometry. An attempt was made, as a test for consistency, to correlate computer results with the approximations developed for scaling pressure and expulsion time. Pressure P and distance of expulsion, Z, were taken from each problem at a time equal to 0.469 of the time at which maximum pressure occurred, t_m, in order to compare results at the approximate midpoint of the principal range of interest. Input conditions are summarized in Table XI. In the table A is the cross-sectional area of the heated section, q_1 is the power entering coolant, and m_0 is the initial mass of coolant to be vaporized and expelled. One additional parameter, c, is needed for the scaling relationships. The parameter c is the change in heat content of the coolant divided by the change in vapor pressure: it is a function of the ratio of heated coolant mass to total coolant mass as well as material properties.

Table XI. Basic Input Conditions

Problem	A (cm^2)	m_0 (gm)	q_1 (MW)	Problem	A (cm^2)	m_0 (gm)	q_1 (MW)
1	13.67	122.5	30.27	6	43.1	13,860	0.194
2	1.57	34.8	0.2168	7	43.1	15,560	15.0
3	0.886	34.8	0.1084	8	43.1	14,510	23.3
4	1.57	34.8	0.1084	9	43.1	14,510	23.3
5	43.1	13,690	0.0586				

Initial pressure P_0 is 1 atm for all problems except 9, for which P_0 = 5 atm.

Figure 9 is a graph of the computed time at 0.469 t_m versus the quantity

$$1.74\sqrt{\frac{m_0^2 cZ}{Aq_1}},$$

the approximation equation for expulsion time. The factor 1.74 is a proportionality constant obtained from a reference problem. Similarly, Figure 10 is a graph of computed pressure at 0.469 t_m as a function of

$$1.80\sqrt{\frac{q_1^2 Z}{Ac^2 m_0}} + P_0,$$

the approximation equation for maximum pressure. As before, 1.80 is a proportionality constant obtained from a reference problem.

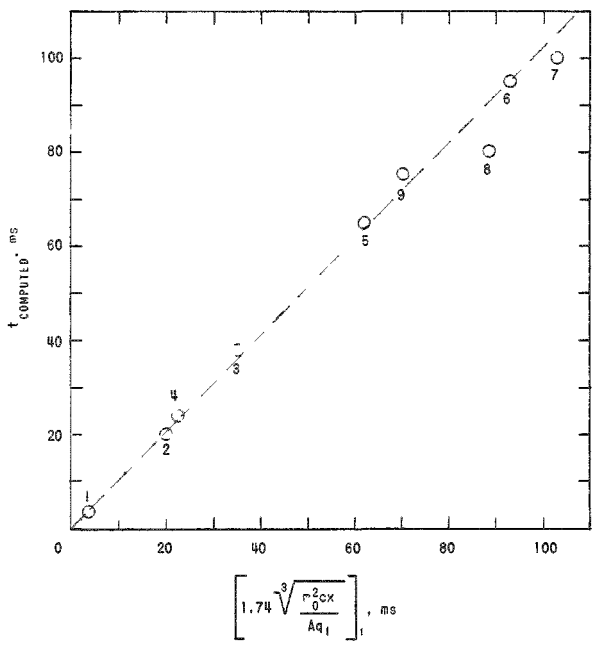

Figure 9. Computed versus Approximated Expulsion Times.

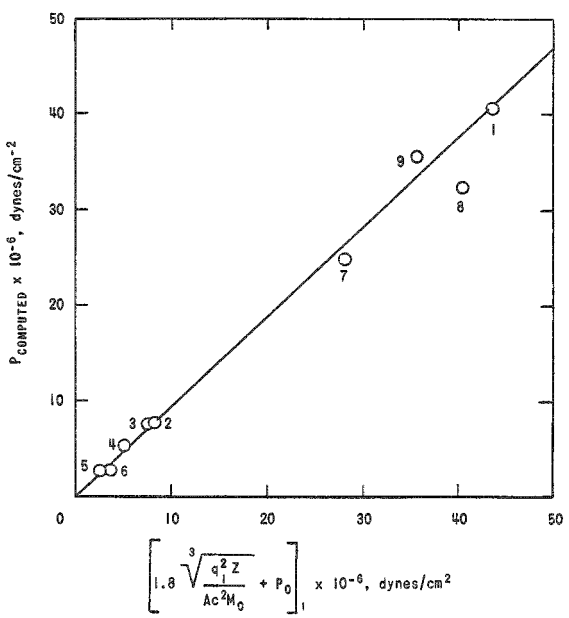

Figure 10. Computed versus Approximated Maximum Pressures.

It appears from the figures that there is a reasonable degree of consistency for a wide range of input conditions between the results obtained from the computer code and the approximation method.

Figure 11 is a graph of the axial displacement of liquid coolant versus time. The graph indicates the extent to which Z is proportional to t^3. This t^3 dependency was anticipated from previously derived scaling relationships.

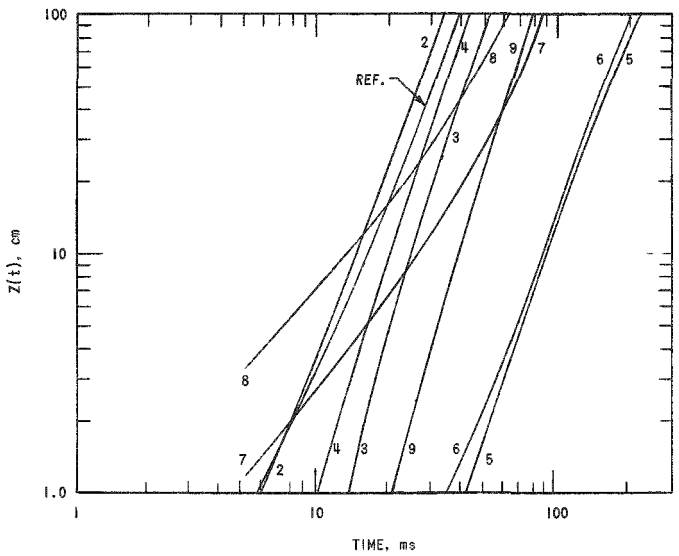

Figure 11

Axial Liquid Displacement versus Time.

2. Meltdown of Pre-irradiated Metallic Elements

The effects of fission product accumulation on fuel meltdown mechanisms is being studied through a continuing program conducted in TREAT. The first series of destructive experiments in transparent capsules on pre-irradiated specimens has been run and awaits post-mortem examination (see Monthly Progress Report for November 1963, ANL-6808, p. 73).

Samples 1 and 2 of the series were pre-irradiated, sodium-bonded, stainless steel-clad, 6% enriched EBR-II fuel-pin prototypes. The high-speed motion films taken during the reactor transients show fuel-pin failures which are consistent with the results indicated by previous meltdown of pre-irradiated samples in opaque capsules. Figure 12 illustrates the sequence of failure of sample 2, in a series of clipped single-frame photographs of the EBR-II fuel pin during the exposure. The successive frames were selected for representative clarity and visual resolution, rather than for time base indication.

In clip 1, the EBR-II fuel pin is shown just prior to failure, with the characteristic spiral warp of the element in response to the separator wire restraint. Clips 2, 3, and 4 show the multiple initial failures of the cladding, and the relatively slow emission of thin jets of opaque gas. The nature and origin of this gas is still unknown. Clips 5, 6, and 7 show the familiar violent emission of sodium vapor from the cladding, characteristic of massive pin failure.

Samples 3 and 4 were pre-irradiated, Zircaloy-clad, 10% enriched, APDA Fermi-A fuel pins. Figure 13 illustrates the failure sequence of sample 4. As in the meltdown of the EBR-II fuel, the first indications of failure of the Fermi element were multiple thin jets of an opaque gas, as

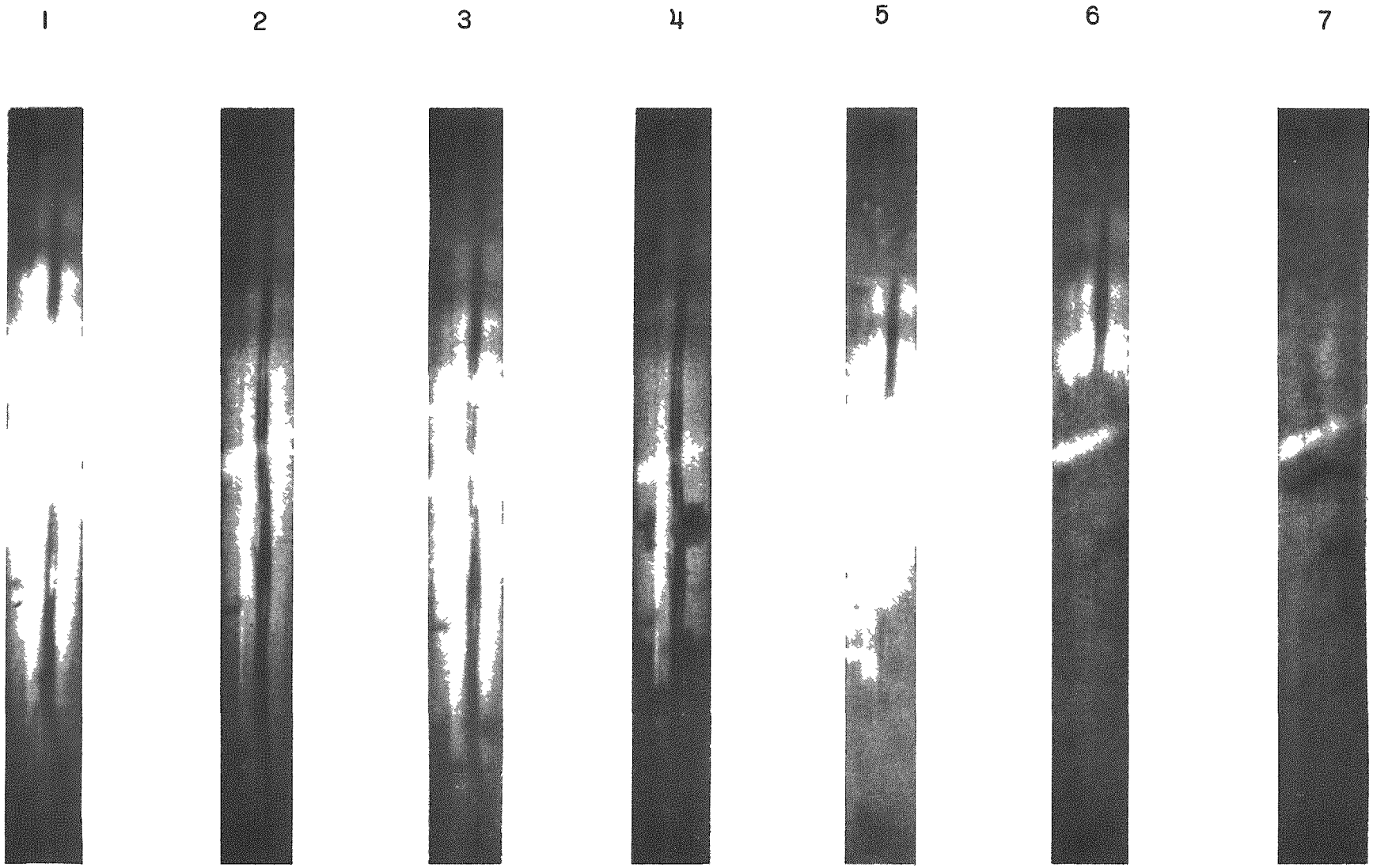

Figure 12. Failure of Pre-irradiated, Sodium-bonded, Stainless Steel-clad EBR-II Fuel Pin, during Meltdown Transient in TREAT.

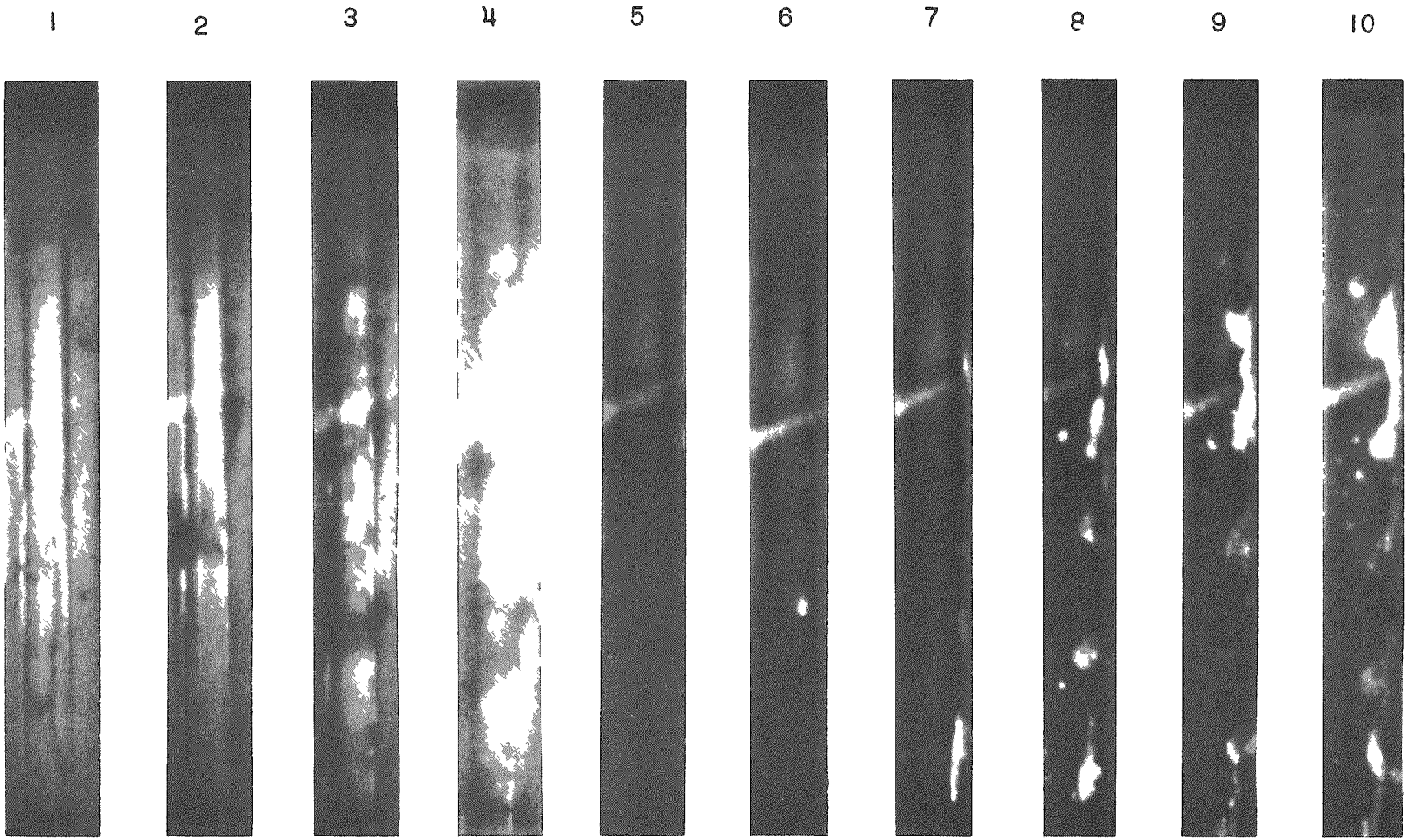

Figure 13. Failure of Pre-irradiated, Zircaloy-clad, APDA Fermi Fuel Pin during Meltdown Transient in TREAT.

shown in clips 2, 3, and 4. The gaseous emission completely obscured the sample (see clip 5) but, apparently of limited volume, the emission seemingly thinned to permit viewing the massive failure and movement of molten fuel and fuel fragments, as shown in clips 7-10.

The similarity of the gas emitted from the metallurgically bonded Fermi fuel pin to the first vapor emitted by the sodium-bonded EBR-II pin in color, viscosity, and relative density, suggests that the gas may be an accumulation of fission products, which precedes the sodium vapor in escaping the breeched EBR-II fuel cladding.

VI. PUBLICATIONS

Papers

STUDY OF THE a-B PHASE TRANSFORMATION IN PLUTONIUM USING ULTRASONICS

R. G. Peterson and Moshe Rosen

J. Acoust. Soc. Am. 35, 1883 (November 1963) Abstract

MATERIALS FOR ARGONNE NATIONAL LABORATORY SODIUM-COOLED REACTORS

R. E. Macherey, W. R. Simmons, and R. A. Noland

IMD Spec. Report Ser. No. 12, Vol. 9, Nuclear Metallurgy AIME, New York, 1963. pp. 57-114

IRRADIATION BEHAVIOR OF REFRACTORY-ALLOY-CLAD PLUTONIUM ALLOYS

W. N. Beck, J. H. Kittel, and R. Carlander

Trans. ANS 6, 375-376 (November 1963)

TECHNIQUES FOR THE FABRICATION OF ULTRA-THIN METALLIC FOILS

Frank J. Karasek

Nucl. Sci. Eng. 17(3) 365-370 (November 1963)

SEPARATION AND SPECTROPHOTOMETRIC DETERMINATION OF TECHNETIUM IN FISSIUM

R. J. Meyer, R. P. Larsen, and R. D. Oldham

Proc. 6th Conf. on Analytical Chemistry in Nuclear Reactor Technology, held at Gatlinburg, Tennessee, October 9-11, 1962. TID-7655, p. 191. Abstract

THE SCATTERING OF FAST NEUTRONS FROM NATURAL URANIUM

A. B. Smith

Nuclear Physics 47, 633-651 (1963)

DISINTEGRATION OF THE DEUTERON IN A COULOMB FIELD

Raymond Gold and Calvin Wong

Phys. Rev. 132(6), 2586-2599 (December 15, 1963)

ALGORITHM 218 - KUTTA MERSON

Phyllis Lukehart

Comm. Assoc. Computing Mach 6(12), 737-738 (December 1963)

CERTIFICATION OF ALGORITHM 118 - REVERSION OF SERIES (Henry E. Fettis, Comm. ACM, 1962)

Henry C. Thacher, Jr.

Comm. Assoc. Computing Mach. 6(12), 745 (December 1963)

THE CONTROL OF FAST REACTORS; CURRENT METHODS AND FUTURE PROSPECTS

W. B. Loewenstein

IAEA Symp. on Physics and Material Problems of Reactor Control Rods, Vienna, November 11-15, 1963. Intern. Atomic Energy, Vienna, 1963. Abstracts of Papers. SM-46/15

ANL Reports

ANL-6550 THE MANUFACTURE OF SUPPLEMENTAL DEPLETED FUEL RODS FOR FCF STARTUP
N. J. Carson, Jr., H. F. Jelinek, and A. B. Shuck

ANL-6622 DEVELOPMENT AND MANUFACTURE OF FUEL, BLANKET, AND THERMOCOUPLE RODS FOR THE EXPERIMENTAL BREEDER REACTOR I, CORE IV
W. R. Burt, Jr., A. G. Hins, R. M. Mayfield, and A. B. Shuck

ANL-6651 SWELLING OF ALUMINUM-CLAD ALUMINUM-PLUTONIUM ALLOYS ON POSTIRRADIATION ANNEALING
B. A. Loomis

ANL-6659 BREEDING-GAIN SPECIMENS FOR EBR-I CORE IV
A. B. Shuck, A. G. Hins, W. R. Burt, and R. A. Beatty

ANL-6665 IRRADIATION AND POSTIRRADIATION ANNEALING OF SOME ALUMINUM-BASE FUELS
C. F. Reinke

ANL-6670 POSTIRRADIATION EXAMINATION OF EBR-I CORE-IV PROTOTYPE FUEL RODS
R. Carlander, J. H. Kittel, and R. J. Dunworth

ANL-6678 PRELIMINARY IRRADIATIONS OF PuC AND UC-PuC
J. H. Kittel, L. A. Neimark, R. Carlander, O. L. Kruger, and R. C. Lied

ANL-6702 HEAT CAPACITY STUDIES OF URANIUM AND URANIUM-FISSIUM ALLOYS
Howard Savage and Richard D. Seibel

ANL-6706 IDAHO DIVISION SUMMARY REPORT, October 1961 through September 1962

ANL-6712 VARIABLY CURING RESINS FOR MOUNTING METALLOGRAPHIC SAMPLES
O. L. Kruger, J. P. Hughes, and F. J. Schmitz

ANL-6721 A PERFORMANCE ANALYSIS OF THE EBWR AT VARIOUS POWER LEVELS
Alfred A. Nentwich

ANL-6775 PERFORMANCE CHARACTERISTICS OF EBWR FROM 0-100 MWT
E. A. Wimunc, M. Petrick, W. C. Lipinski, and H. Iskenderian

ANL-6779 TWO-PHASE CRITICAL FLOW WITH APPLICATION TO LIQUID-METAL SYSTEMS (MERCURY, CESIUM, RUBIDIUM, POTASSIUM, SODIUM, AND LITHIUM)
Hans K. Fauske